Picoeukaryotes of the Micromonas genus: sentinels of a warming ocean

David Demory, Anne-Claire Baudoux, Adam Monier, Nathalie Simon, Christophe Six, Pei Ge, Fabienne Rigaut-Jalabert, Dominique Marie, Antoine Sciandra, Olivier Bernard, et al.

Picoeukaryotes of the *Micromonas* genus: sentinels of a warming ocean

David Demory[1,2,3,*], Anne-Claire Baudoux[4], Adam Monier[5], Nathalie Simon[4], Christophe Six[4], Pei Ge[4], Fabienne Rigaut-Jalabert[6], Dominique Marie[4], Antoine Sciandra[2], Olivier Bernard[3,*], and Sophie Rabouille[2,*]

[1]School of Biology, Georgia Institute of Technology, Atlanta, GA, USA
[2]Sorbonne University, UPMC Univ Paris 06, INSU-CNRS, UMR 7093, Laboratoire Océanographique de Villefranche, 181 Chemin du Lazaret, 06230 Villefranche-sur-mer,France
[3]INRIA BIOCORE UCA, BP93, 06902 Sophia-Antipolis Cedex, France
[4]Sorbonne University, UPMC Univ Paris 06, INSU-CNRS, UMR 7144, Station Biologique de Roscoff, 29680 Roscoff, France
[5]Biosciences, University of Exeter, Exeter, UK
[6]Sorbonne University, UPMC Univ Paris 06, CNRS, Fédération de Recherche FR2424, Station Biologique de Roscoff, 29680 Roscoff, France
[*]Corresponding author: david.demory@biosci.gatech.edu; olivier.bernard@inria.fr; srabouille@obs-vlfr.fr

May 15, 2018

Abstract

Photosynthetic picoeukaryotes in the genus Micromonas show among the widest latitudinal distributions on Earth, experiencing large thermal gradients from poles to tropics. Micromonas comprises at least four different species often found in sympatry. While such ubiquity might suggest a wide thermal niche, the temperature response of the different strains is still unexplored, leaving many questions as for their ecological success over such diverse ecosystems. Using combined experiments and theory, we characterize the thermal response of eleven Micromonas strains belonging to four

species. We demonstrate that the variety of specific responses to temperature in the Micromonas genus makes this environmental factor an ideal marker to describe its global distribution and diversity. We then propose a diversity model for the genus Micromonas, which proves to be representative of the whole phytoplankton diversity. This prominent primary producer is therefore a sentinel organism of phytoplankton diversity at the global scale. We use the diversity within Micromonas to anticipate the potential impact of global warming on oceanic phytoplankton. We develop a dynamic, adaptive model and ran forecast simulations, exploring a range of adaptation time scales, to probe the likely responses to climate change. Results stress how biodiversity erosion depends on the ability of organisms to adapt rapidly to temperature increase.

Introduction

The Intergovernmental Panel for Climate Change (IPCC) stressed unequivocal warming of the climate system. Their Fifth Report anticipates rises in the global mean surface temperature by the end of 21st century ranging from 0.3-1.7 °C (RCP2.6) to 2.6-4.8 °C (RCP8.5) [1]. Oceans participate in buffering the increasing emissions of greenhouse gases, thus modulating the warming; in addition to the chemical equilibration of gas species between the atmosphere and dissolved phases, phytoplankton is an important contributor of carbon remediation through CO_2 sequestration in the ocean [2]. Should dramatic shifts occur in species biodiversity and distribution following temperature increases [3, 4], the resilience of ecosystems could severely be impaired. The likely responses of ecosystems to such rapid temperature changes are at the core of debates, with worrisome consequent impacts on oceanic biogeochemical cycles and feedbacks on the climate system [5].

Phytoplankton live in a thermally fluctuating environment that constrains growth capacity [3, 6, 7]. The temperature growth response of phytoplankton varies widely, both between and within taxa. Phenotypic plasticity determines the ability to acclimate to short-term environmental variations while genetic adaptations characterize evolutionary processes under long-term changes. These features will provide, or not, each species with the capacity to survive in a given biotope and to evolve by modifying their thermal niche. Since temperature depends on latitude [8, 9, 10, 11], it is therefore a probable driver of niche partition in the oceans, creating large-scale biogeographic patterns [12]. Hence, the structure and diversity of phytoplankton communities could partly reflect observed trends in the global temperature [6, 7].

Temperature-related interspecific distributions have been studied for the whole phytoplankton community [3] but few studies explored intragenus diversity [13, 14]. *Micromonas* species have emerged as emblematic representative of the

eukaryotic pico-phytoplankton communities, thriving in a variety of ecosystems from polar to tropical waters [15, 16, 17, 18]. They often dominate phytoplankton in coastal environments [19], where their major contribution to primary production influences the biogeochemical cycles [20]. In the past decade, phylogenetic analyses identified several distinct genetic lineages within *Micromonas* and have suggested that this genus was composed of cryptic species [21, 22, 23, 24]. Four species have now been formally described [25]. *Micromonas* spp. may co-occur at various latitudes, but were found to occupy different temporal or depth niches within their sympatric ranges [23].

As observed for picocyanobacteria [26, 13], the temperature response of such a widely distributed and phylogenetically diverse eukaryote is expected to vary between *Micromonas* species. The interspecific diversity within the genus *Micromonas*, the number of characterized strains, and abundant omics data make it a relevant model organism to both explore the impact of temperature on latitudinal distribution and diversity of phytoplankton, and to shed light on the mechanisms that drive phytoplankton thermal responses in the ocean. We therefore studied the thermotolerance and thermal growth response of eleven *Micromonas* strains in the laboratory under controlled conditions (hereafter referred as experimental strains) and we derived a mathematical model that describes the impact of temperature on growth rate. With this model, we uncover the logic that lies behind the observed distribution of species and their co-occurrence; we also reveal the existence of thermotypes within the genus. We extrapolated the thermal response to a set of 46 additional strains from the Roscoff Culture Collection (hereafter referred as collection strains), observed in various oceanic regions, showing that temperature is the main driver of diversity and distribution in this genus. Then, we developed a predictive model of niche partition to characterize *Micromonas* interspecific diversity, which we successfully validated against the Tara Oceans dataset [27], making it a plausible prediction tool. We demonstrated that *Micromonas* distribution is a relevant and accurate proxy of the whole phytoplankton community distribution. More than a sentinel of the ocean biogeochemistry as previously suggested by Worden and colleagues [28], *Micromonas* is a probe for global warming. To explore how phytoplankton communities may respond to a future, warmer ocean, we ran the niche partition model under IPCC Sea Surface Temperature (SST) projections, adding an evolutionary model that accounts for the potential adaptation of growth to temperature changes.

Results and discussion

Micromonas strains feature distinct physiological responses to temperature

To estimate the temperature tolerance and growth responses of the four described *Micromonas* species, we selected three strains of *M. commoda*, *M. bravo* and *M. pusilla* as well as two strains of *M. polaris*. We measured their exponential growth rate after being grown for two months between 4°C and 35°C (41.52 ± 30.61 generations on average, Supplementary Table 2) depending on the strain origin. To increase the accuracy in the temperature response estimation, the experimental protocols followed the recommendations given in [29, 30] (see Methods). The chosen strains, obtained from the Roscoff Culture Collection (RCC), were originally isolated from contrasted thermal niches of the Atlantic, Pacific and Artic basins (Figure 1a, Supplementary Figure 3 and Supplementary Table 1). All showed a typical [31, 32] asymmetric growth response to temperature, which we characterized by four cardinal growth parameters: T_{min} and T_{max}, respectively the minimum and maximum temperatures for growth; μ_{opt}, the maximum specific growth rate obtained at the optimum temperature T_{opt} (Figure 1b). Overall, the *Micromonas* genus was able to grow over the thermal range tested, but with diverse and specific responses for each strain, depicted by distinct cardinal parameters (Supplementary Table 6). Temperature stimulates enzymatic processes and metabolic rates, but also accelerates cell mortality [33]. In the suboptimal range ($T < T_{opt}$), enzymatic activity increases more than mortality in response to increasing temperatures. At T_{opt} this balance between metabolic activity and mortality is optimized and yields the highest observed net growth rate. At supra optimal temperatures ($T > T_{opt}$), the denaturation of key metabolic enzymes, like rubisco [34] and the thermolability of Photosystem II [35] are exacerbated, along with an increase of the membrane damages [36] ; as a consequence, the net growth rate sharply decreases with temperature up to the maximal growth temperature the strain can withstand (T_{max} at which μ is null).

Several patterns appeared when comparing the growth response to the annual average SST ($\overline{T}_S$) at the site where each strain was isolated. Strains isolated in locations where $\overline{T}_S$ was above 19.7°C (RCC 299 and RCC 829) were able to grow up to high temperatures (T_{max} = 32.6±0.02 and 37.0±0.12°C, respectively); they showed a high μ_{opt} (1.1±0.05 to 1.3±0.07d^{-1}, respectively) at an elevated optimum T_{opt} temperature (26.3±1.01 to 29.3±1.2°C, respectively). Strains isolated in regions where the average SST fluctuates between 16.0 and 18.0°C presented a lower optimal growth rate (0.9±0.03d^{-1}) at T_{opt} = 22.6 ± 3.08 °C) and maintained positive growth from 4.2±5.6°C to 28.7±4.63°C. In strains isolated at sites with

an average temperature between 10.1 and 13.6°, μ_{opt} still reached 0.87±0.08d^{-1} at T_{opt}=23.8±0.62°C and cells demonstrated an ability to grow over a very wide temperature range (from -0.7±7.46°C to 29.4±1.55°C). Last, Arctic strains (RCC2306 and RCC2257) revealed both the narrowest growth temperature range (-7.0±0° to 15.1±0°C) and lowest growth rates (0.45±0.03 d^{-1}) at 7.5±0°C.

In Summary, the four formerly described *Micromonas* species exhibited specific temperature tolerance and growth optima in vitro and their according response parameters were related to the thermal environment from which the strains were isolated. Model parameters T_{min}, and to a lesser extent T_{max}, are difficult to accurately estimate [32]. Since measurements for temperatures close to T_{min} (but slightly higher) and close to T_{max} (but slightly lower) are generally rare, they must be extrapolated from a mathematical model. These parameters also bracket the thermal niche, i.e. the breadth of the thermal response. For instance, it appears that Arctic strains showed a much narrower niche: they were more stenotherm compared to the other strains.

The *Micromonas* genus includes six thermotypes: evidence from the most recent phylogeny.

The phylogenetic analysis of the 57 *Micromonas* 18S DNA sequences from the eleven experimental and 46 collection strains highlighted the existence of six distinct phylogenetic groups (see Methods and Supplementary Figure 2). To identify whether they were associated with specific thermal conditions in the ocean, we analyzed available data of average SST in areas where *Micromonas* spp. were sampled. We computed a non-metric dimensional scaling (NMDS) of the thermal environment dataset (see Methods). The significant ordination (stress = 0.004) identified six different distributions in the thermal environment, from warmer, low latitudes to colder, high latitudes, that showed a good match with the phylogenetic tree (Figure 2a and Supplementary Figure 3), demonstrating that the thermal niche of *Micromonas* was related to its phylogenetic affiliation. *M. polaris* and *M. pusilla* strains occupied respectively a narrow and wide thermal niche while *M. bravo* and *M. commoda* each included two distinct groups. One isolated from a warmer (lower latitude; warm group) and one isolated in a colder (higher latitudes; cold group) environment (Figure 2a and Supplementary Figure 3).

There are few examples in the literature of latitudinal segregation within eukaryotic phytoplankton genera [37, 38]. For example, the global distribution of *Ostreococcus* clades, a picoeukaryote close to *Micromonas* is related to temperature but first seems to discriminate rather coastal, high-light adapted clades from more oceanic, low-light adapted clades [39]. In agreement with the hypothesis of

Foulon *et al.* [23], our experimental and phylogenetic results showed that a niche segregation within *Micromonas* did occur that is consequent to thermal, group-specificities and which compels with the recently identified, four known species. The present analysis further revealed the existence of two thermotypes within both *M. commoda* and *M. bravo* species, making a total of six distinct *Micromonas* thermotypes.

Establishing a thermal response model for *Micromonas* thermotypes

To obtain a better appraisal of the thermal response of strains, we looked for possible correlations between cardinal growth parameters and environmental features where strains had been isolated. Among the tested descriptors of the SST dynamics, the average surface temperature at the isolation site ($\overline{T}_S$) best correlated with the cardinal temperature. For T_{min}, the latitude was also included in the regression (Table 1 and Supplementary Figure 6a). The optimal growth rate (μ_{opt}) increased with $\overline{T}_S$, following the Eppley's hypothesis of a faster growth rate at warmer temperatures [40]. The maximal growth temperature (T_{max}) and the optimal growth temperature (T_{opt}) were also both positively correlated with $\overline{T}_S$, suggesting that environmental temperature featured the upper tolerance window of strains. The minimal temperature of growth (T_{min}) had the lowest correlation with the environmental temperature (Supplementary Figure 6b), as also reported by [41] for different phytoplankton species. We found that the minimal growth temperature T_{min} best correlated (negatively) with a combination of the yearly average temperature $\overline{T}_S$ and latitude (Lat, Supplementary Figure 7). In the end, the growth response (μ_{opt}, T_{min}, T_{opt} and T_{max}) of cultured strains can thus accurately be predicted from the thermal environments ($\overline{T}_S$) and latitude from which they were isolated, using the relations defined in Table 1. Last, statistically significant correlations were also found between cardinal parameters (Supplementary Figure 8). In particular, the optimal temperature of growth (T_{opt}) linearly correlated with the maximal temperature of growth (T_{max}) by a factor close to 1, as previously highlighted for a wide range of bacterial species [42].

The relationships between cardinal growth parameters and environmental temperatures deduced from the culture experiments (Table 1) were used to extrapolate the cardinal parameters of 46 additional *Micromonas* collection strains, using the latitude and average annual temperature of their isolation site (Table 1 and Supplementary Table 9). This data set confirmed a segregation of the four species into six different thermotypes. To deduce a representative thermal response for each thermotype, we randomly chose 100,000 values within the confidence interval

of the cardinal parameters of each group and ran Monte Carlo simulations of the related thermal responses (see Methods). The Bernard and Rémond (BR) model was then fitted to each bundle of simulated responses [32] to obtain the average thermal response curve representative of each thermotype (Figure 2b and Supplementary Figures 9, 10 and 11). Last, we calibrated the envelope curve, inspired from [43], on the *Micromonas* genus, by fitting the BR model [32] to the set of (T_{opt},μ_{opt}) obtained for each thermotype (see Methods and Figure 2b).
With the narrowest thermal niche (23.04 ± 2.42°C), *M. polaris* was the most stenotherm species. *M. commoda* cold and *M. bravo* cold showed very similar responses at colder temperatures but discriminated in regard to the optimum growth rate and maximum temperature. Their thermal niche of 25.42 ± 3.75°C and 27.10 ± 0.91°C, respectively, was representative of cold-temperate environments. Contrary to the cold species, and although they both live in warmer biotopes, the warm thermotype of species *M. commoda* and *M. bravo* showed very distinct thermal niches (34.00 ± 1.19°C and 26.02 ± 5.11, respectively). Last, *M. pusilla* was found in both cold- and warm-temperate areas and showed an intermediate thermal response compared to the other *Micromonas* species, with a thermal niche of 28.85 ± 5.32°C. With the most variable response to temperature, *M. pusilla* did not seem to speciate into different thermotypes; yet it clearly differentiated from other groups and would be the most eurytherm.

Tara Oceans dataset validates the global segregation of thermotypes.

To validate our hypothesis that temperature is a key factor that greatly influences *Micromonas* biogeography over a yearly period, we retrieved the 18S V9 metabarcodes dataset obtained in the frame of Tara Oceans [27](Figure 3). Read abundance data assigned to each of the *Micromonas* thermotypes were identified across 47 stations, spanning 6 marine regions with different thermal environments: Mediterranean Sea, Red Sea, Indian Ocean, South Atlantic Ocean, Southern Ocean and South Pacific Ocean (Figure 3a). Using an NMDS ordination method, we first compared the relative abundance of each *Micromonas* thermotype at sampling stations (see Methods and Figure 3b) to the physicochemical environmental conditions observed along the Tara Oceans circumnavigation. The presence of *Micromonas* species was better explained by temperature (R^2 = 0.48, *p*-value $<$ 0.001) than by nutrient availability, mixing, or geographical location. To a lower extent, nutrients (NO_2+NO_3, PO_4 and NO_2; $R^2 < 0.23$, *p*-value $<$0.032), Chl *a* concentration ($R^2 = 0.1710$, *p*-value = 0.003) and mixed layer depth (MLD;$R^2 =$ 0.13, *p*-value = 0.03) also explained significantly the *Micromonas* assemblages along the transect. Temperature is thus the strongest descriptor of the change in diversity between Tara Oceans stations.

We then compared the relative abundance of thermotypes at all stations in relation to yearly SST (Figure 3c). A very clear thermal separation appeared between the two *M. commoda* thermotypes, further supporting our identification of two distinct thermotypes. *M. commoda* cold was most abundant in waters with temperature below 20°C and rarely found beyond 25°C, while *M. commoda* warm mostly occurred between 25°C and 30°C and was completely absent at stations where temperatures were below 15°C. Species *M. bravo* was less often observed than *M. commoda* and showed overlapping distributions of its two warm and cold thermotypes, which we believe was due to the large thermal niche of the warm thermotype spreading over that of the more restrained, cold thermotype (Figure 2). A non-distinct distribution (Figure 3c) in the Tara Oceans data could also suggest that the evolution of the two *M. bravo* thermotypes was more recent. Species *M. polaris* was observed only at stations with T<10°C with highest abundances near 0°C, validating the psychrophilic characteristics of this thermotype. Species *M. pusilla* was only found at a few stations compared to *M. commoda* and *M. bravo*; it was observed from 12°C to 30°C with a maximum abundance above 25°C. This distribution may well be related to the fact that its thermal response is close to the barycenter of the whole *Micromonas* thermal response (average parameters: $\overline{T_{opt}} = 21.26$, $\overline{\mu_{opt}} = 0.84$ and $\overline{(T_{max} - T_{min})} = 28.34$). The reported occurrences of this species at low concentrations all around the globe [23, 44] could support the idea that it plays a "seed bank" role, acting as a dormancy stage of *Micromonas* compared to other species [45]. Interestingly, Foulon *et al.* [23] also suggested a possible niche partition over depth, along a light gradient that may explain the low concentration of *M. pusilla* in the Tara Oceans dataset. In the end, temperature is a sufficient parameter to describe the latitudinal segregation of *Micromonas* between Tara Oceans stations. The current typology of Tara Oceans (they mainly are open ocean areas), does not allow to fully assess a possible effect of nutrients [46].

Influence of temperature on the intragenus diversity of *Micromonas* assemblages

To further understand the thermal niche partition of *Micromonas* at the global scale, we proposed a simple index to relate *Micromonas* intragenus diversity to the global average SST (Figure 4 and Supplementary Figure 12). We computed an interspecific *Micromonas* diversity index (Shannon derived/based) from the growth response of a given thermotype i to a considered local temperature T

according to the equation:

$$H(T) = \sum_{i=1}^{n} \mathcal{D}_i \ln(\mathcal{D}_i) \text{ with } \mathcal{D}_i = \frac{\mu_i(T)}{\sum_{i=1}^{n} \mu_{opt,i}} \quad (1)$$

Where $\mathcal{D}_i$ is the distribution index, $\mu_i(T)$ is the growth rate at the temperature T, and $\mu_{opt,i}$ is the optimal growth for the thermotype i. We compared $H(T)$ to a Shannon-like index for the *Micromonas* genus at each Tara Oceans sampling station using the proportion of each *Micromonas* thermotype OTU in the total counted *Micromonas* OTU and the local SST annual average (Figure 4a and b). Based on the calculated diversity index $H(T)$, we were able to qualitatively predict the *Micromonas* intragenus diversity estimated from the Tara Oceans V9-18S dataset (Spearman test: ρ = 0.417, p-value = 0.0035), thereby validating our theoretical developments. The diversity index followed a fluctuating trend through the cruise path characterized by different thermal environments (Figure 3a).

When running the *Micromonas* diversity model at the global scale (Figure 4c and Supplementary Figure 13), the predicted diversity was minimal at the poles (Lat $>$ 60°N and $>$50°S) and at the equator (between 20°N and 20°S), especially in the Indian Ocean and the Pacific Ocean (Figure 4c). Maximum diversity levels were found from 20 to 60°N and from 20 to 40°S. We used the relationship between the phytoplankton diversity as calculated by Thomas and colleagues [3] and our *Micromonas* diversity to normalize our diversity index within Thomas's scale (see Methods). Our simulated global *Micromonas* diversity was point by point compared to the whole phytoplankton potential diversity calculated by Thomas and collaborators [3] (Figure 4d). We found a very strong relationship between the two diversity patterns (R^2_{adj} = 0.97, p-value < 0.05; see Methods and Supplementary Figure 15). This result strongly suggests that the diversity between *Micromonas* thermotypes, at mesoscale and on a yearly basis, is representative of the whole phytoplankton community. It likely explains the overall success of the genus to colonize very contrasted biotopes [19, 23]. *Micromonas* could thus serve as a relevant marker of the biodiversity of phytoplankton communities. The term "sentinel", originally proposed by [28] to depict the role of *Micromonas* on ocean biogeochemistry is all the more relevant considering this genus reflects the pattern of the whole phytoplanktonic community and can help to better anticipate the impact of ocean warming.

Diversity evolution in a warmer ocean: a matter of the adaptation time scale

To explore the impact of future temperature changes on phytoplankton diversity, we investigated its evolution using SST projections over the period 2001-2100. To account for the adaptation capability [4, 47], we proposed a very simple adaptive model. This model assumes that the evolution time scale is related to the local doubling time $\frac{\ln(2)}{\mu_i(T)}$ of each thermotype i. Adaptation is thus faster for the warm thermotypes in warm environments. The adaptation dynamics describes the evolution of the cardinal temperatures (T_{min}, T_{opt} and T_{max}) from their present value to their value at the end of the century. The evolution rate is estimated according to the characteristic number of generations Na required to adapt to a different temperature, *i.e.* to shift each cardinal (i.e. represented by the character "c") temperature T_c to its asymptotic value T_c^*, defined as the evolutionary equilibrium given the changes of the surface temperature T at each time step (Supplementary Figure 16). The evolution dynamics of each cardinal parameter $T_{c,i}$ is described by a simple first order equation:

$$\frac{dT_{c,i}}{dt} = \frac{N_i(T(t))}{Na}(T^*_{c,i}(T(t)) - T_{c,i}(t)) \quad (2)$$

Where $N_i(T(t)) = \frac{\mu_i(T(t),T_{c,i})}{\ln(2)}$, with $\mu_i(T(t), T_{c,i}(t))$ the growth rate at the temperature T, calculated using the set of cardinal parameters $T_{c,i}$ for the thermotype i.

We ran this model for different Na, from fast adaptation scales (Na < 100 generations) to slow adaptation scales ($Na = 10^6$ generations) and calculated the evolution of thermotypes diversity between the present period (2001 to 2010) and future period (2091 to 2100, Figure 5). We considered two realistic evolution hypotheses to describe the dichotomy between specialist and generalist species: the Specialist-generalist hypothesis with constant thermal niche width (Figure 5a and b) and the Specialist-generalist hypothesis with dynamical thermal niche [48] (Figure 5c and d - see Methods). Over the 21st century, SST will globally increase by 2 to 3°C over the whole ocean surface and up to 5°C around 45° N, with the exception of the highest latitudes, which may see a slight decrease in their average temperature (Supplementary Figure 17).

Similar erosion patterns were found for both specialist-generalist hypotheses that showed diversity losses between 40°S to 40°N. At latitudes higher than 40°, we found possible gains in biodiversity, regardless of the adaptation scenario and the evolution hypothesis. At these latitudes, for most phytoplankton species, the optimum temperature (T_{opt}) is higher than the average environmental temperature

($\overline{T}_S$). With a fast adaptation scenario, thermal traits follow the thermal environment and T_{opt} remains above $\overline{T}_S$, each thermotype keeps its thermal niche and diversity is not affected. In contrast, thermal traits will not change fast enough in a slow adaptation scenario; $\overline{T}_S$ gets closer to T_{opt}, and each thermotype ends up with a fitness that is out of phase with the thermal environment (Supplementary Figure 18). While these conditions are still favorable for growth, they typically increase the diversity. Finally, for the adaptation scenario where the thermal niche can increase, it gives more chance for a species to adapt faster even for a higher change in the thermal environment (Supplementary Figure 19). At latitudes lower than 40°, ocean warming will drive a decrease in phytoplankton diversity, with a mitigation of diversity losses tightly dependent on the adaptation time scale and similar for both hypotheses (Figure 5a and c). Slow adaptation scenarios lead to an important diversity erosion compared to fast adaptation scenarios, suggesting that the adaptation time scale is a key parameter in the mitigation of diversity loss and matters far more than the strategy of adaptation itself. In areas most vulnerable to diversity erosion (Supplementary Figure 20 and 21), faster adaptation reduces the average diversity erosion from 4.5 species lost per latitude degree (slow adaptation) to one species lost or even 2 species gained per latitude (fast adaptation, Figure 5b and d). Thermal adaptation performed within 200-300 generations might be sufficient to mitigate the impacts of climate change on phytoplankton diversity. In contrast, an adaptation scale beyond 10^4 generations will not counteract the deep impacts of climate change on phytoplankton diversity.
The adaptation time scale of the thermal tolerance of different phytoplankton taxa has been closely related to their respective thermal environments (measured with T_{opt} or the Net Primary Production) [49, 50, 51, 52]. Phytoplankton taxa that ought to efficiently adapt to temperature are encountered in highly variable thermal environments [49], typically found at latitudes beyond 40°, where we found positive change in future diversity. These regions are also the main areas of CO_2 mitigation and carbon export in the ocean [2, 53]. The deeper alteration of phytoplankton diversity in the tropics might prove less critical for the efficiency of the biological pump at the global scale. Future research should be addressed to understand the impact of microbial diversity on carbon export [54].

Conclusion

This study describes niche partitioning in the marine pico-phytoplankton *Micromonas*. We showed that this genus evolved into different thermotypes that discriminate according to their sensitivity to temperature. Our model predictions were validated by *in situ* data from the Tara Oceans scientific expedition and suggest that temperature is a robust descriptor of *Micromonas* distribution at

mesoscale and on a yearly basis. The diversity within this genus is highly correlated to the diversity pattern of the whole phytoplankton community. It is crucial to dedicate specific efforts to monitor the evolution of this sentinel genus in order to keep a real-time high fidelity picture of the phytoplankton diversity across the oceans. It is likely that *Micromonas* genus comprises even more thermotypes. More refined laboratory assessments including more thermotypes, should they exist, would enhance the representation of the global phytoplankton distribution. In particular, new experiments with smaller temperature increments and including more points at low and high temperatures would provide with a much higher resolution in the predicted capabilities and better assessment of T_{min} and T_{max}. Although decisive, the ability of phytoplankton to adapt in a warming ocean is the yet uncertain parameter. Adaptation is directly or indirectly affected by a variety of factors such as local nutrient availability, predation, virus lysis, mixing regime, etc. All of them are affected by the local physical dynamics and will also be impacted by global warming. More research is thus required to understand the adaptation mechanisms of this sentinel organism, and especially the adaptive dynamics of the different thermotypes. Such an approach will progressively refine the picture of phytoplankton evolution in a changing ocean with the possibility to more rapidly detect tipping points.

Methods

A graphic abstract of the overall, scientific approach is provided in Supplementary Figure 1.

Growth measurements and thermal response model

Culture conditions. Eleven *Micromonas* spp. strains were selected from the RCC for the laboratory experiments. We chose strains representative of all the currently known species and according to their isolation site, to consider a range of organisms found along a latitudinal gradient (Supplementary Table 1). Cells were grown in batch cultures in ventilated polystyrene flasks (Nalgene, Rochester, NY, USA) in K-Si medium [55]. Cultures were maintained in temperature-controlled chambers (Aqualytic, Dortmund, Germany) at different temperatures (4, 7.5, 9.5, 12.5, 20, 25, 27.5, 30 and 32.5°C) for two months (see Supplementary Table 2 for the number of generations) under a 12h:12h light-dark cycle with 100 μmol photons m^{-2} s^{-1} provided by fluorescent tubes (Mazda 18WJr/865).

Growth response curves. Cell concentration was determined on fresh samples using flow cytometry according to [56]. The maximum cell growth rate (μ_{max})

was calculated as the slope of the linear regression relating cell concentration logarithm *vs.* time observed during the exponential phase of growth. The Cardinal Temperature Model with Inflection (BR model) from [32] was used to estimate the optimal temperature of growth (T_{opt}) at which the growth rate is optimal (μ_{opt}), and the minimal and maximal temperatures of growth (T_{min} and T_{max}) at which $\mu = 0$. The growth $\mu(T)$ at temperature T is described as follows:

$$\mu(T) = \begin{cases} 0 & \text{for } T < T_{min} \\ \mu_{opt}.\phi(T) & \text{for } T_{min} < T < T_{max} \\ 0 & \text{for } T > T_{max} \end{cases} \quad (3)$$

$$\text{where } \phi(T) = \frac{(T - T_{max})(T - T_{min})^2}{(T_{opt} - T_{min})[(T_{opt} - T_{min})(T - T_{opt}) - (T_{opt} - T_{max})(T_{opt} + T_{min} - 2T)}$$

Selection of the thermal growth response model. Number of models exist that represent the response of phytoplankton strains to temperature; we selected the one we believe to be the most relevant for the purpose of the present study. We first short-listed the most appropriate models after the two recent reviews of [30] and [57]. Grimaud and colleagues [30] discussed the strengths and limitations of several thermal response models in regard to four criteria: the fit quality, the easiness of calibration, the biological interpretation of parameters, and the applicability to phytoplankton growth. They convincingly argued that the BR (Eq. 3, [32]) and Eppley-Norberg (Eq. 4, [58]) models presented the overall best performances. Following the analysis from [57], we also considered the Boatman model (Eq. 5, [59]) and we calibrated all three models to our growth measurements (Supplementary Figure 4 and 5).

$$\mu(T) = \left[1 - \left(\frac{T - T_{opt}}{w}\right)^2\right] ae^{bT} \text{ where } w = abs(T_{max} - T_{min}) \quad (4)$$

$$\mu(T) = \mu_{max} \left[sin\left(\pi \frac{T - T_{min}}{T_{max} - T_{min}}\right)^a\right]^b \quad (5)$$

We then computed an Akaike Information Criterion (AIC) and a Bayesian Information Criterion (BIC) for each model (Supplementary Table 5) according to the following equations:

$$AIC = 2k - 2ln(MSE) \quad (6)$$

$$BIC = -2ln(AIC) + kln(n) \quad (7)$$

Where k is the number of model parameters to be estimated, MSE the Mean Square Error between measured and predicted growth rates and n the number of data points. These two criteria provide with an estimation of the relative quality of the models tested. Being an increasing function of MSE and k, the BIC is a selection criterion between models. The BR model yielded the smallest criteria and, in this regard, represented the best model tested to represent the growth response to temperature in *Micromonas*, in agreement with the findings of [30] for other phytoplankton species.

Phylogenetic tree reconstruction and evolutionary placements.

Sequence alignment. 18S amplicon sequences from *Micromonas* RCC strains were aligned to a reference Mamiellophyceae sequence alignment. This reference alignment spans the rDNA operon and was originally used to describe the phylogenetic relationships amongst Mamiellophyceae genera (Marin and Melkonian, 2010). The reference alignment was trimmed to represent only the 18S rDNA region; long Micromonas RCC 18S amplicons (> 1000 nt; n = 35) were added to this alignment using MAFFT v7 [60]. The resulting alignment was then edited using the mask from the original alignment annotation [24] and was composed of a total of 2158 sites.

Phylogenetic tree reconstruction. The edited alignment was used for maximum-likelihood (ML) tree reconstructions. The best ML tree was identified from 100 independent tree reconstructions. All ML reconstructions were run using RAxML v8 [61] with the HKY85+G+I model, which was determined as the best-fit model of nucleotide substitution with jModelTest v2 [62] and by both the Akaike and Bayesian information criteria. Node supports of the resulting phylogenetic tree were determined using 1000 non-parametric bootstrap replicates. Bayesian inferences were conducted using BEAST v2 [63] using the HKY85+I+G with a log-normal, relaxed molecular clock and default priors. A total of 4 MCMC chains of 10^6 generations were conducted, and a 25% 'burnin' value was applied on the resulting tree set. The iTol web-server [64] was used to generate vector scalable graphic rendering.

Evolutionary placements. RCC 18S amplicon sequences shorter than 1000 nt (n = 24) were placed onto the ML phylogeny using the Evolutionary Placement Algorithm (EPA) implemented in RAxML v8 [65]. Short RCC sequences were aligned with MAFFT v7 against the previously generated updated reference Mamiellophyceae 18S alignment (i.e., composed of reference Mamiellophyceae and long RCC amplicon sequences). The aligned short sequences were then placed

onto the reference phylogeny using RAxML in EPA mode with the HKY85+I+G model.

Thermal niche partitioning analysis.

Thermal environment dataset. Using SST from the National Oceanic and Atmospheric Administration's (NOAA), we built a dataset gathering the environmental temperatures at the isolation site of the eleven experimental and 46 *Micromonas* collection strains referenced in the RCC. At each strain's isolation site, we retrieved the yearly average SST ($\overline{T}_S$), minimum SST (T_S^-), maximal SST (T_S^+) and thermal amplitude ($T_S^+ - T_S^-$) corresponding to a 10-year average (2005 to 2014).

Thermal environment analysis. To identify possible correlation of isolated strains to temperature, a non-metric dimensional scaling (NMDS) was realized on a Euclidean distance matrix computed on the thermal environment dataset (T_S^-, $\overline{T}_S$, T_S^+, $T_S^+ - T_S^-$) using the R package vegan [66]. The stress value is the measure of how well the NMDS configuration represents the dissimilarities and is referred as the Kruskal stress [67].

Relation between strains and environmental temperatures. Relationships between environmental temperatures (T_S^-, $\overline{T}_S$, T_S^+, $T_S^+ - T_S^-$), latitude of the isolation site (Lat) and the species cardinal parameters (T_{min},T_{opt},T_{max} and μ_{max}) were calculated for the eleven experimental strains that were grown in the laboratory. We tested simple and multiple linear regression models and chose the best relationship according to a high $R^2_{adjusted}$ and p-value < 0.05. Best relationships were obtained with $\overline{T}_S$ and were used to determine cardinal parameters of all other 46 collection strains that were not experimentally tested but referenced in the RCC.

Thermotypes construction. For each thermotype, we computed 100,000 growth *vs.* temperature curves through a Monte Carlo procedure with the BR model [32] and cardinal parameters of the i-th thermotype randomly taken from the parameter distributions (assuming a gaussian repartition of the parameters in the interval $[p^* - 2\sigma, p^* + 2\sigma]$ where p^* are the parameters value). In order to ensure a biological coherence in the random samples of the cardinal parameters, the μ_{opt} parameter is generated slightly differently. An Eppley model is used to link μ_{opt} and T_{opt} [40]:

$$\mu_{opt} = a.e^{b.T_{opt}} \tag{8}$$

Where parameters a and b are obtained from the best fit with all the strains of the thermotype (Supplementary Table 7). The values of μ_{opt} for a random strain are then directly deduced from random values of T_{opt} using this model.
Finally, we used the BR model to get the average thermal response and its standard deviation for each thermotype.
The optimal growth response envelope [43] for the whole *Micromonas* genus was calculated with a BR curve calibrated on a data set consisting in 57 couples (T_{opt},μ_{opt}) from the eleven experimental strains and the 46 collection strains. Moreover, the decreasing part of the curve was constrained with 8 couples (T,$\mu(T)$) simulated from the *M. commoda* Warm thermotype model for temperatures equally distributed in the (T_{opt},T_{max}) interval for this thermotype. The increasing part of the curve was also constrained with eleven couples (T,$\mu(T)$) simulated from the *M. polaris* model for temperatures equally distributed in the (T_{min},T_{opt}) interval for this species.

Tara Oceans

Tara Oceans V9 dataset analysis. Molecular and contextual data from the Tara Oceans project were retrieved from PANGAEA [68]. The Tara Oceans V9-18S dataset [27] is available both at the barcode level (non-redundant sequences) and clustered at the Swarm/operational taxonomic unit level [69]. *Micromonas*-like V9-18S barcode sequences were retrieved based on the original taxonomic classification from the Tara Oceans consortium, which was conducted with the Protist Ribosomal Reference database [70] for the protist barcode subset. The resulting 1084 non-redundant barcodes classified as *Micromonas*-like, and which represented a total of 95755 occurrences across the V9-18S Tara Oceans sampling (334 samples from 47 stations), were then re-classified using a phylogenetic placement procedure. The non-redundant *Micromonas*-like V9-18S barcodes were aligned against a reference Mamiellophyceae alignment using the same methodology than for the short 18S amplicon sequences from the *Micromonas* RCC strains, as aforementioned. The V9-18S barcode sequences were then placed onto the Mamiellophyceae and RCC reference tree using RAxML EPA with the HKY85+I+G model. Based on the placement of the Tara Oceans barcode onto the *Micromonas* reference subtree, the corresponding taxonomic information (thermotype level) was assigned to the environmental barcode.

Thermotypes inside the Tara Oceans V9 dataset. To explore the impact of temperature on species occurrence, we computed an NMDS on a Bray-Curtis distance matrix calculated from a community matrix of *Micromonas* species abundance per station (expressed in percentage of barcodes) with the R package "vegan" [66].

Results display a cloud of sampling stations from the different oceanic basins, discriminating surface and deep chlorophyll maximum (DCM); the closer proximity of stations, in terms of Bray-Curtis distances, expresses their similarities in their 18S diversity. We then fitted environmental variables (nutrients, temperature and mixed layer depth) and total chlorophyll *a* abundance on the ordination space with the vegan function $envfit$ in vegan package [66] with p-value based on 999 permutations was used to assess the significance of the fit.
The *Micromonas* distribution for each thermotype was computed against yearly SST (from NOAA) for each Tara Oceans station. We then computed Loess regressions with polynomial fitting to illustrate the temperature patterns with the R package "ggplot2" [71].

Global temperature response and diversity index

Global SST dataset. We used global SST data from the Copernicus Marine Environment Monitoring Service (product: GLOBAL_REP_PHYS_001_013) to calculate monthly averages SST in the period 1993 - 2012 at the global scale.

Species distribution as a function of temperature. Cardinal parameters (T_{min}, T_{opt}, T_{max}) and optimum growth rate μ_{opt} for each thermotype i were used to calculate the growth rate $\mu_i(T)$ for each temperature T using the BR model [32]. Then, normalized distribution $\mathcal{D}_i(T)$ of each thermotype was calculated following the equation: $\mathcal{D}_i(T) = \frac{\mu_i(T)}{\sum_{i=1}^{n} \mu_{opt,i}}$ for each temperature T of the global ocean surface. Remark that this normalisation removes the effect of other factors which also influence net growth at the same location (nutrients, light, predations, etc.).

Diversity index. To get a diversity index, we computed 10,000 thermal distribution via a Monte Carlo procedure for each species (Supplementary Figure 13). We then computed an averaged and standard deviation of a Shannon-like based interspecific diversity index within the *Micromonas* genus according to Eq. 1 (Supplementary Figure 14) and compared it with a Shannon diversity index based on Tara Oceans V9 dataset thermotypes relative abundance:

$$H_{TARA}(s) = \sum_{i=1}^{n} E(s,i) ln(E(s,i)) \tag{9}$$

Where $E(s,i)$ is the number of barcodes for the *Micromonas* thermotype i at the station s. The Tara Oceans dataset was used along the transect from station 4 to 125 [27]. The spatial distance between stations was calculated as a distance as the crow flies. In addition, we compare the Shannon-like base interspecific diversity

index (Eq. 1) calculated for *Micromonas* (H_M) to the diversity index calculated by Thomas and colleagues for the phytoplankton (H_P) with a linear regression model ($R^2_{adj} = 0.95$ and p-value < 0.5):

$$H_P = 83.21 H_M + 65.05 \tag{10}$$

Then, we used Eq. 10 to quantify the diversity in the same index as the Thomas *et al.* study [3] (Supplementary Figure 15).

Cardinal parameters adaptation model

Cardinal Parameters Evolution. We studied the evolution of diversity in a warmer ocean with a dynamical model of the thermal growth response over the period 2001 to 2100. Projections of future, global temperature regimes were obtained from the NOAA GFDL CM2.1 [72, 73] driven with the SRES A2 emissions scenario [74]. This dataset spans from 2001 to 2100 and was also used by Thomas and colleagues [3].

First, we computed the evolution of cardinal parameters $T_{c,i}$ (T_{min},T_{opt} and T_{max}) for each thermotype i depending on the temperature $T(t, l, L)$ with t the year, l the latitude and L the longitude. The evolution of cardinal parameters follows Eq. 2, which is parameterized by the number of generations Na required to adapt to a different temperature (Supplementary Figure 16):

$$\frac{dT_{opt,i}}{dt} = \frac{N_i(T(t))}{Na}(T^*_{opt,i}(T(t)) - T_{opt,i}(t)) \tag{11}$$

$$\frac{dT_{max,i}}{dt} = \frac{N_i(T(t))}{Na}(T^*_{max,i}(T(t)) - T_{max,i}(t)) \tag{12}$$

Where $T^*_{opt,i}$ and $T^*_{max,i}$ are computed from the derivative of the relationships in Table 1 depending on the local temperature $T(t, l, L)$:

$$\frac{dT^*_{opt,i}}{dt} = 0.84\frac{dT(t,l,L)}{dt} \tag{13}$$

$$\frac{dT^*_{max,i}}{dt} = 0.77\frac{dT(t,l,L)}{dt} \tag{14}$$

The evolutive minimal temperature of growth was computed contingent to the

evolution hypothesis:

$$T^*_{min,i} = \begin{cases} T^{ini}_{min,i} + T^*_{max,i} - T^{ini}_{max,i} & \text{Constant thermal niche} \\ \\ \frac{dT_{min,i}}{dt} = \frac{N_i(T(t))}{Na}(T^*_{min,i}(T(t)) - T_{min,i}(t)) & \text{Dynamical model (Eq. 2)} \end{cases} \tag{15}$$

Where $T^{ini}_{min,i}$ and $T^{ini}_{max,i}$ are the initial value of $T_{min,i}$ and $T_{max,i}$ respectively at time $t = 2001$ and $T^*_{min,i}$ is computed from the derivative of the relationships in Table 1 depending on the local temperature $T(t, l, L)$:

$$\frac{dT^*_{min,i}}{dt} = -0.92\frac{dT(t,l,L)}{dt} \tag{16}$$

We constrained $T^*_{min,i}$ and $T^*_{max,i}$ by the envelope curve [43] of the *Micromonas* genus (Figure 2b) that represents its evolution boundaries.

Second, we calculated $\mu_{opt,i}$ at $T_{opt,i}$ with the BR model calibrated with the cardinal parameters of the envelope curve.

Third, we calculated the related growth rate $\mu_i(T)$ of each thermotype i depending on its cardinal parameters $T_{c,i}$ at temperature $T(t, l, L)$ following the BR model [32].

Third, we calculated the diversity for the present (2001 to 2010 - H_{now}) and future (2091 to 2100 - H_{future}) periods following the Eq. 1 averaged on 10 years and expressed as the diversity index used by Thomas and colleagues [3] with the Eq. 10.

Diversity erosion. We performed this cardinal parameter evolution framework for different values of Na, from fast ($Na < 100$ generations) as highlighted by [50, 51] to slow ($Na = 10^9$) adaptation kinetics. This slow time scale corresponds to two to six months in the lab, which means a time scale in the range of years in the natural environment (assuming $\mu = 0.2$ day^{-1} as a typical growth rate in the sea). For long-term evolution, we refer to a time scale slower than climate change. We call slow evolution an evolution with a typical adaptation kinetics with a millennium, which means $Na = 10^6$ generations for an average growth rate of 0.2 day^{-1}. We then calculated a diversity erosion index representing the loss of diversity along the latitude gradient with the equation:

$$H_{erosion}(l) = \frac{h_L}{L_{max}} \sum_{L=0}^{L_{max}} (H_{now}(l, L) - H_{future}(l, L)) \tag{17}$$

With L the longitude and l the latitude, L_{max} the maximal longitude of the dataset ($n = 359.7$) and h the longitude resolution ($h_L = 0.1$).

The averaged latitudinal erosion ($\overline{H_{erosion}}$) per latitude was calculated as follows:

$$\overline{H_{erosion}} = \frac{h_l}{n} \sum_{l=l_{min}}^{l_{max}} (H_{erosion}(l)) \tag{18}$$

With l the latitude, l_{min} and l_{max} the minimum and maximum latitude of the dataset ($l_{min} = -82$ and $l_{max} = 90$), h_l the latitude resolution ($h_l = 0.1$) and n the $H_{erosion}$ vector's length. A negative erosion signifies a diversity gain.
The tipping point (p) of the $\overline{H_{erosion}}$ vs. Na curve was calculated as the inflection point following the equation:

$$p = \max\left(\frac{d\overline{H_{erosion}}}{dNa}\right) \tag{19}$$

References

[1] Pachauri RK, Allen MR, Barros VR, Broome J, Cramer W, Christ R, *et al.* (2014). Climate change 2014: synthesis Report. Contribution of working groups I, II and III to the fifth assessment report of the intergovernmental panel on climate change. IPCC.

[2] Sabine CL, Feely RA, Gruber N, Key RM, Lee K, Bullister JL, *et al.* (2004). The Oceanic Sink for Anthropogenic CO_2. Science 305: 367–371.

[3] Thomas MK, Kremer CT, Klausmeier CA and Litchman E. 2012. A Global Pattern of Thermal Adaptation in Marine Phytoplankton. Science 338: 1085–1088.

[4] Irwin AJ, Finkel ZV, Muller-Karger FE and Troccoli Ghinaglia L. 2015. Phytoplankton adapt to changing ocean environments. PNAS 112: 5762–5766.

[5] Reid PC, Fisher AC, Lewis-Brown E, Meredith MP, Sparrow M, Andersson AJ, *et al.* 2009 Impacts of the oceans on climate change. Advances in Marine Biology 56: 1–150.

[6] Sunagawa S, Coelho LP, Chaffron S, Kultima JR, Labadie K, Salazar G., *et al.* 2015. Structure and function of the global ocean microbiome. Science 348: 1261359.

[7] Farrant GK, Doré H, Cornejo-Castillo FM, Partensky F, Ratin M, Ostrowski M, *et al.* 2016. Delineating ecologically significant taxonomic units from global patterns of marine picocyanobacteria. PNAS 113: E3365-E3374.

[8] Rutherford S, D'Hondt S and Prell W. 1999. Environmental controls on the geographic distribution of zooplankton diversity. Nature 400: 749–752.

[9] Fuhrman JA. 2009. Microbial community structure and its functional implications. Nature 459:193–199.

[10] Tittensor DP, Mora C, Jetz W, Lotze HK, Ricard D, Berghe EV, *et al.* 2010. Global patterns and predictors of marine biodiversity across taxa. Nature 466:1098–1103.

[11] Jun Sul W, Oliver TA, Ducklow HW, Amaral-Zettler LA and Sogin ML. 2013. Marine bacteria exhibit a bipolar distribution. PNAS 110: 2342–2347.

[12] Wiens JJ. 2011. The niche, biogeography and species interactions. Philosophical Transactions of the Royal Society B: Biological Sciences 366: 2336–2350.

[13] Pittera J, Humily F, Thorel M, Grulois D, Garczarek L, and Six C. 2014. Connecting thermal physiology and latitudinal niche partitioning in marine *Synechococcus*. The ISME Journal 8: 1221–1236.

[14] Martiny AC, Ma L, Mouginot C, Chandler JW, Jeremy W and Zinser ER. 2016. Interactions between Thermal Acclimatation, Growth Rate, and Phylogeny Influence *Prochlorococcus* Elemental Stoichiometry. PloS one 11: e0168291.

[15] Lovejoy C, Vincent WF, Bonilla S, Roy S, Martineau MJ, Terrado R, *et al.* 2007. Distribution, phylogeny, and growth of cold-adapted picoprasinophytes in Arctic seas. Journal of Phycology 43: 78-89.

[16] Worden AZ and Not F. 2008. Ecology and diversity of picoeukaryotes. Microbial Ecology of the Oceans, Second Edition: 159–205.

[17] Monier A, Sudek S, Fast NM and Worden AZ. 2013. Gene invasion in distant eukaryotic lineages: discovery of mutually exclusive genetic elements reveals marine biodiversity. The ISME Journal 7: 1764–1774.

[18] Monier A, Comte J, Babin M, Forest A, Matsuoka A and Lovejoy C. 2015. Oceanographic structure drives the assembly processes of microbial eukaryotic communities. The ISME Journal 9: 990-1002.

[19] Not F, Latasa M, Marie D, Cariou T, Vaulot D and Simon N. 2004. A Single Species, *Micromonas pusilla* (Prasinophyceae), Dominates the Eukaryotic Picoplankton in the Western English Channel. Applied and Environmental Microbiology 70: 4064–4072.

[20] Massana R. 2011. Eukaryotic Picoplankton in Surface Oceans. Annual Review Microbiology 65: 91–110.

[21] Guillou L, Eikrem W, Chrétiennot-Dinet MJ, Le Gall F, Massana R, Romari K, *et al.* 2004. Diversity of Picoplanktonic Prasinophytes Assessed by Direct Nuclear SSU RDNA Sequencing of Environmental Samples and Novel Isolates Retrieved From Oceanic and Coastal Marine Ecosystems. Protist 155: 193–214.

[22] Slapeta J, Lopez-Garcia P and Moreira D. 2006. Global Dispersal and Ancient Cryptic Species in the Smallest Marine Eukaryotes. Molecular Biology and Evolution 23: 23–29.

[23] Foulon E, Not F, Jalabert F, Cariou T, Massana R and Simon N. 2008. Ecological niche partitioning in the picoplanktonic green alga *Micromonas pusilla*: evidence from environmental surveys using phylogenetic probes. Environmental Microbiology 10: 2433–2443.

[24] Marin B and Melkonian M. 2010. Molecular phylogeny and classification of the Mamiellophyceae class. nov. (Chlorophyta) based on sequence comparisons of the nuclear- and plastid-encoded rRNA operons. Protist 161: 304–336.

[25] Simon N, Foulon E, Grulois D, Six C, Desdevises Y, Latimier M, *et al.* 2017. Revision of the genus *Micromonas* Manton et Parke (Chlorophyta, Mamiellophyceae), of the type species *M. pusilla* (Butcher) Manton & Parke and of the species *M. commoda* van Baren, Bachy and Worden and description of two new species based on the genetic and phenotypic characterization of cultured isolates. Protist 168: 612–635.

[26] Johnson ZI, Zinser ER, Coe A, McNulty NP, Woodward EMS and Chisholm SW. 2006. Niche partitioning among *Prochlorococcus* ecotypes along ocean-scale environmental gradients. Science 311: 1737–1740.

[27] De Vargas C, Audic S, Henry N, Decelle J, Mahé F, Logares R, *et al.* 2015. Eukaryotic plankton diversity in the sunlit ocean. Science 348: 1261605.

[28] Worden AZ, Lee JH, Mock T, Rouzé P, Simmons MP, Aerts AL,*et aL.* 2009. Green evolution and dynamic adaptations revealed by genomes of the marine picoeukaryotes *Micromonas*. Science 324: 268–272.

[29] Boyd PW, Rynearson TA, Armstrong EA, Fu F, Hayashi K, Hu Z, *et al.* 2013. Marine phytoplankton temperature versus growth responses from polar to tropical waters-outcome of a scientific community wide study. PLoS One 8: e63091.

[30] Grimaud GM, Mairet F, Sciandra A and Bernard O. 2017. Modeling the temperature effect on the specific growth rate of phytoplankton: a review. Reviews in Environmental Science and Bio/Technology 16: 625–645.

[31] Raven JA and Geider RJ. 1988. Temperature and Algal Growth. The New Phytologist 110: 441–461.

[32] Bernard O and Rémond B. 2012. Validation of a simple model accounting for light and temperature effect on microalgal growth. Bioresource Technology 123: 520–527.

[33] Serra-Maia R, Bernard O, GonÃğalves A, Bensalem S, Lopes F, Influence of temperature on *Chlorella vulgaris* growth and mortality rates in a photobioreactor. Algal Research 18: 352–359.

[34] Salvucci ME and Crafts-Brandner SJ. 2004. Inhibition of photosynthesis by heat stress: The activation state of Rubisco as a limiting factor in photosynthesis. Physiologia Plantarum 120: 179–186.

[35] Rokka A, Aro EM, Herrmann RG, Andersson B and Vener AV. Dephosphorylation of photosystem II reaction center proteins in plant photosynthetic membranes as an immediate response to abrupt elevation of temperature. Plant Physiology 123: 1525–1536.

[36] Los DA and Murata N. 2004. Membrane fluidity and its roles in the perception of environmental signals. Biochimica et Biophysica Acta - Biomembranes 1666: 142–157.

[37] Cuvelier ML, Allenc AE, Monier A, McCrow JP, Messie M, Tringed SG, *et al.* 2010. Targeted metagenomics and ecology of globally important uncultured eukaryotic phytoplankton. Proceedings of the National Academy of Sciences 107: 14679-14684.

[38] Monier A, Worden AZ and Richards TA. 2016. Phylogenetic diversity and biogeography of the Mamiellophyceae lineage of eukaryotic phytoplankton across the oceans. Environmental microbiology reports 8: 461–469.

[39] Demir-Hilton E, Sudek S, Cuvelier ML, Gentemann CL, Zehr JP and Worden AZ. 2011. Global distribution patterns of distinct clades of the photosynthetic picoeukaryote *Ostreococcus*. The ISME Journal 5: 1095–1107.

[40] Eppley RW. 1972. Temperature and phytoplankton growth in the sea. Fishery Bulletin 70: 1063–1085.

[41] Chen B. 2015. Patterns of thermal limits of phytoplankton. Journal of Plankton Research 37: pp 285–292.

[42] Rosso L, Lobry JR and Flandrois JP. 1993. An unexpected correlation between cardinal temperatures of microbial growth highlighted by a new model. Journal of Theoretical Biology 162: 447–463.

[43] Grimaud GM. 2016. Modelling the temperature effect on phytoplankton: from acclimation to adaptation. Doctoral dissertation, University Nice Sophia Antipolis.

[44] Baudoux AC, Lebredonchel H, Dehmer H, Latimier M, Edern R, Rigaut-Jalabert F, *et al.* 2015. Interplay between the genetic clades of *Micromonas* and their viruses in the Western English Channel. Environmental Microbiology Reports 7: 765–773.

[45] Lennon JT and Jones SE. 2011. Microbial seed banks: the ecological and evolutionary implications of dormancy. Nature Reviews Microbiology 9: 119–130.

[46] Botebol H, Lelandais G, Six C, Lesuisse E, Meng A, Bittner L, *et al.* 2017. Acclimatation of a low iron adapted *Ostreococcus* strain to iron limitation through cell biomass lowering. Scientific Report 7: 327.

[47] Grimaud GM, Le Guennec V, Ayata SD, Mairet F, Sciandra A and Bernard O. 2015. Modelling the effect of temperature on phytoplankton growth across the global ocean. IFAC-PapersOnline 48: 228–233.

[48] Stinchcombe JR, Function-valued Traits Working Group and Kirkpatrick M. 2012. Genetics and evolution of function-valued traits: understanding environmentally responsive phenotypes. Trends in Ecology and Evolution 27: 637–647.

[49] Huertas IE, Rouco M, Lopez-Radas V and Costas E. 2011. Warming will affect phytoplankton differently: evidence through a mechanistic approach. Proceedings of the Royal Society B 278: 3534–3543.

[50] Padfield D, Yvon-Durocher G, Buckling A, Jennings S and Yvon-Durocher G. 2016. Rapid evolution of metabolic traits explains thermal adaptation in phytoplankton. Ecology Letters 19: 133–142.

[51] Bonnefond H, Grimaud G, Rumin J, Bougaran G, Talec A, Gachelin M, *et al.* 2017. Continuous selection pressure to improve temperature acclimation of *Tisochrysis lutea*. PloS one 12: e0183547.

[52] Schaum CE, Barton S, Bestion E, Buckling A, Garcia-Carreras B, Lopez P, *et al.* 2017. Adaptation of phytoplankton to a decade of experimental warming linked to increased photosynthesis. Nature Ecology & Evolution 1: 0094.

[53] Lutz MJ, Caldeira K, Dunbar RB and Behrenfeld MJ. 2007. Seasonal rhythms of net primary production and particulate organic carbon flux to depth describe the efficiency of biological pump in the global ocean. Journal of Geophysical Research 112: C10.

[54] Guidi L, Chaffron S, Bittner L, Eveillard D, Larhlimi A, Roux S, *et al.* 2016. Plankton networks driving carbon export in the oligotrophic ocean. Nature 532: 465.

Material references

[55] Keller MD, Selvin RC, Claus W and Guillard RRL. 1987. Media for the culture of oceanic ultraphytoplankton. Journal of Phycology 23: 633–638.

[56] Marie D, Brussaard CPD, Thyrhaug R, Bratbak G and Vaulot D. 1999. Enumeration of Marine Viruses in Culture and Natural Samples by Flow Cytometry. Applied and Environmental Microbiology 65: 45–52.

[57] Low-Decarie E, Boatman TG, Bennet N, Passfield W, Gavalas-Olea A, Siegel P and Geider RJ. 2017. Predictions of response to temperature are contingent on model choice and data quality. Ecology and Evolution 7: 10467–10481.

[58] Norberg J. 2004. Biodiversity and ecosystem functioning: a complex adaptive systems approach. Limnology and Oceanography 49: 1269–1277.

[59] Boatman TG, Lawson T and Geider RJ. 2017. A key marine diazotroph in a changing ocean: The interacting effects of temperature, CO2 and light on the growth of *Trichodesmium erythraeum* IMS101. PLoS one 12: e0168796.

[60] Katoh K and Standley DM. 2013. MAFFT multiple sequence alignment software version 7: improvements in performance and usability. Molecular Biology and Evolution 30: 772–780.

[61] Stamatakis A. 2014. RaxML version 8: a tool for phylogenetic analysis and post-analysis of large phylogenies. Bioinformatics 30: 1312–1313.

[62] Darriba D, Taboada GL, Doallo R and Posada D. 2012. jModelTest 2: more models, new heuristics and parallel computing. Nature Methods 9: 772–772.

[63] Bouckaert R, Heled J, Kuhnert D, Vaughan T, Wu CH, Xie D, *et al.* 2014. BEAST 2: A Software Platform for Bayesian Evolutionary Analysis. PLoS Computational Biology 10: e1003537.

[64] Letunic I and Bork P. 2011. Interactive Tree Of Life v2: online annotation and display of phylogenetic trees made easy. Nucleic Acids Research 39: W475-W478.

[65] Berger SA and Stamatakis A. 2012. Aligning short reads to reference alignments and trees. Bioinformatics 27: 2068–2075.

[66] Oksanen J, Kindt R, Legendre P, Minchin PR, O'hara RB, Simpson GL, *et al.* 2016. vegan: Community Ecology Package. R package version 2.4-0, available at (https://CRAN.R-project.org/package=vegan).

[67] Kruskal JB. 1964. Multidimensional scaling by optimizing goodness of fit to a nonmetric hypothesis. Psychometrika 29: 1-27.

[68] Pesant S, Not F, Picheral M, Kandels-Lewis S, Le Bescot N, Gorsky G, *et al.* 2015. Open science resources for the discovery and analysis of Tara Oceans data. Scientific Data 2: 150023.

[69] Mahé F, Rognes T, Quince C, de Vargas C and Dunthorn M. 2014. Swarm: robust and fast clustering method for amplicon-based studies. PeerJ 2: e593.

[70] Guillou L, Bachar D, Audic S, Bass D, Berney C, Bittner L, *et al.* 2012. The Protist Ribosomal Reference database (PR2): a catalog of unicellular eukaryote small sub-unit rRNA sequences with curated taxonomy. Nucleic Acids Research 41: D597-D604.

[71] Wickham H. 2016. ggplot2: Elegant Graphics for Data Analysis. Springer.

[72] Griffies SM, Gnanadesikan AWDK, Dixon KW, Dunne JP, Gerdes R, Harrison MJ, *et al.* 2005. Formulation of an ocean model for global climate simulations. Ocean Science 1: 45–79.

[73] Delworth T, Broccoli AJ, Rosati A, Stouffer RJ, Balaji V, Beesley JA, *et al.* 2006. GFDL's CM2 global coupled climate models. Part I: Formulation and simulation characteristics. Journal of Climate 19: 643–674.

[74] Nakicenovic N, Alcamo J, Grubler A, Riahi K, Roehrl RA, Rogner HH and Victor N. 2000. Special report on emissions scenarios: A special report of Working Group III of the Intergovernmental Panel on Climate Change. Nakicenovic N, Swart R, Eds. (Cambridge University Press, Cambridge, UK; Working Group III of the Intergovernmental Panel on Climate Change.

Conflit of interest statement

Authors declare no conflit of interest for this study.

Acknowledgements

We thank members of the RCC for their help and work to maintain many phytoplankton strains in culture. We are also grateful to Mridul Thomas for providing his phytoplankton diversity data [3] and to Keith Paarporn for proofreading the text. Finally, we thank the reviewers and editor for their constructive comments on a previous version of this manuscript. This research was funded by the Inria Project Lab Algae in silico and by the ANR funding agency REVIREC (grant no. 12-BSV7-0006-01).

Author contributions

D.D., A-C.B., O.B., N.S., A.S. and S.R. designed the study. D.D., A-C.B., N.S., P.G., F.R-J. carried out the experiments. D.D. and O.B. carried out the modeling and statistical analyses. D.D. provided the display items. A.M. carried out the phylogenetic and Tara Ocean V9 dataset analysis. C.S. and D.M. helped technically. D.D., O.B. and S.R. wrote the manuscript with contributions from N.S., C.S. and A-C.B.

Figure and Table legends

Figure 1: *Micromonas growth response to temperature. (a) Location of isolation sites of the eleven Micromonas experimental strains used in this study, plotted against yearly average SST for the year 2014 (from NOAA). (b) Growth rate vs. temperature curves for strains isolated in environments with different annual average temperature ($\overline{T}_S$), fitted by the BR model [32]. Error bars are standard deviations ($n \geqslant 3$).*

Table 1: *Linear relationship between cardinal parameters and environmental parameters (average temperature at the surface of isolation site, $\overline{T}_S$, and the latitude, Lat) for the eleven Micromonas experimental strains tested in this study.*

Figure 2: *Original thermal environments and growth response to temperature for Micromonas species. (a) Two-dimensional ordination space derived from a Non-Metric MultiDimensional Scaling (NMDS) procedure displaying the thermal dissimilarities site (T_S^-, $\overline{T}_S$, T_S^+ and $T_S^+ - T_S^-$) between the original isolation sites of the eleven experimental and 46 Micromonas collection strains. The stress value (goodness-of-fit of the NMDS) is inferior to 0.05, indicating high dimensional relationships among samples. (b) Average growth response to temperature for each phylogenetic group computed from 100,000 possible response curves simulated within the ranges observed in each phylogenetic group. The black line represents the overall, optimal growth response envelope [43] of Micromonas computed as μ_{opt} vs. T_{opt}, where μ_{opt} and T_{opt} are given by the average response of each thermotype. The grey shaded area is the standard deviation around μ_{opt}.*

Figure 3: *Micromonas thermotypes relative abundance patterns as estimated from the 18S rRNA V9 region during the Tara Oceans cruise. (a) Map of the Tara Oceans transect (dashed black line)showing station for which 18S rRNA V9 region data were available from Vargas et al. (2015) [27]: Mediterranean Sea (Med S), Red Sea (Red S), Indian Ocean (Ind O), South Pacific Ocean (S Pac O), Southern Ocean (S O) and South Atlantic Ocean (S Atl O). (b) Two-dimensional ordination space derived from an NMDS analysis displaying Bray-Curtis distance between the Micromonas species assemblages of the Tara Oceans stations, fitted by significant environmental variable (p-value < 0.05). The stress value (goodness-of-fit of the NMDS) is 0.15, indicating fair dimensional relationships among samples. (c) Relative abundance of the 6 thermotypes per station, plotted according to yearly SST at station coordinates: data (circles) and polynomial regression (solid line) fitted with the 95% confidence interval (shaded area). Number of observations for the 6 thermotypes are represented in histograms, plotted according to yearly SST at station coordinates.*

Figure 4: *Estimated and predicted interspecific diversity within the Micromonas genus in the global ocean. (a) Estimated and predicted interspecific diversity within the Micromonas genus along the Tara Oceans transect as estimated from the Micromonas OTUs read abundances (blue circles) and as predicted from our diversity model (red circles), fitted by a polynomial regression with a 95% confidence interval. (b) Thermotypes proportions (%) from Tara Oceans dataset for different oceanic regions: Mediterranean Sea (Med S), Red Sea (Red S), Indian Ocean (Ind O), South Pacific Ocean (S Pac O), Southern Ocean (S O) and South Atlantic Ocean (S Atl O). (c) Predicted Shannon diversity index (H) calculated with the equation 1 using annual averages SST (Copernicus Marine Environment Monitoring Service, 1993 to 2012 satellite data). (d) Comparison of the latitudinal average diversity for all phytoplankton (from Thomas et al. 2012. black line) with that estimated by our Micromonas model. Shaded area represents the standard deviation from the mean along latitudes.*

Figure 5: *Micromonas diversity changes in a warming ocean for two evolution hypotheses: (a-b) Specialist-generalist with constant thermal niche and (c-d) Specialist-generalist with dynamical thermal niche. (a-b) Latitudinal averaged diversity erosion calculated as the difference between diversity in present period (2001 to 2010) and future (2091 to 2100). Black line represents the diversity erosion from Thomas et al. 2012, red and blue line are the diversity erosion for the fast adaptation scenario (Na = 100) and slow adaptation scenario (Na = 10^6) respectively. Filled area represent the standard deviation to the mean along latitude. (c-d) Averaged diversity erosion per latitude calculated for different adaptation kinetic (from Na = 1 to Na = 10^6 generations): model results (black circles) and polynomial regression (blue line) fitted. The Tipping point is calculated as the inflexion point for the derivative of blue curve. The 20% loss point is calculated as 20% evolution from the lowest erosion scenario (Na = 1).*

Picoeukaryotes of the *Micromonas* genus: sentinels of a warming ocean

David Demory[1,2,3,*], Anne-Claire Baudoux[4], Adam Monier[5], Nathalie Simon[4], Christophe Six[4], Pei Ge[4], Fabienne Rigaut-Jalabert[6], Dominique Marie[4], Antoine Sciandra[2], Olivier Bernard[3,*], and Sophie Rabouille[2,*]

[1]School of Biology, Georgia Institute of Technology, Atlanta, GA, USA
[2]Sorbonne University, UPMC Univ Paris 06, INSU-CNRS, UMR 7093, Laboratoire Océanographique de Villefranche, 181 Chemin du Lazaret, 06230 Villefranche-sur-mer,France
[3]INRIA BIOCORE, BP93, 06902 Sophia-Antipolis Cedex, France
[4]Sorbonne University, UPMC Univ Paris 06, INSU-CNRS, UMR 7144, Station Biologique de Roscoff, 29680 Roscoff, France
[5]Biosciences, University of Exeter, Exeter, UK
[6]Sorbonne University, UPMC Univ Paris 06, CNRS, Fédération de Recherche FR2424, Station Biologique de Roscoff, 29680 Roscoff, France
[*]Corresponding author: david.demory@biosci.gatech.edu; olivier.bernard@inria.fr; srabouille@obs-vlfr.fr

May 15, 2018

Supplementary Figure 1: *Summary of the scientific approach*

Micromonas thermal responses

1) Thermal response experiments in laboratory

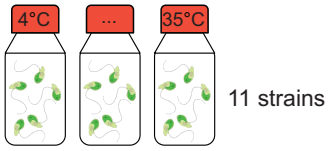

2) BR model fits to obtain cardinal parameters (CP)

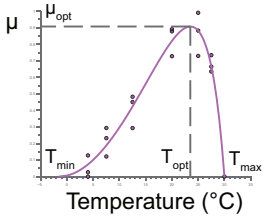

3) Relationships between cardinal parameters (CP) and thermal environment data from NASA

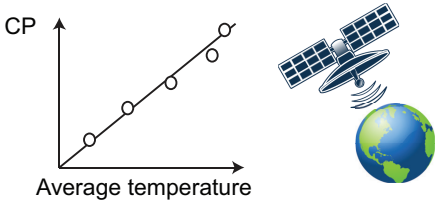

4) Extention of the 11 experimental strains to 46 additional collection strains to create a dataset of temperature response with 57 *Micrmonas* strains.

Thermotype definition

5) Phylogeny from 18S sequences for the RCC *Micromonas* strains

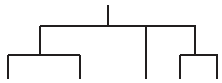

Thermotypes definition thanks to the phylogeny, the thermal response and the thermal environment for each strain with statistical ordination methods

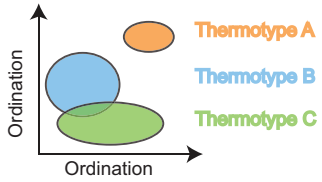

6) Exploration of the Tara Oceans data set to validate our theoretical results

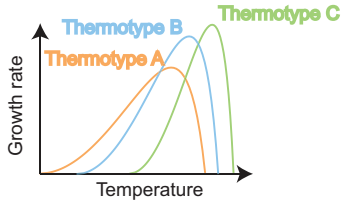

Biogeography

7) Theoretical calculus of the thermotype distribution at the global scale with SST data-set

8) Summary of the distribution with a Shannon like diversity index related to the thermal response of each thermotype

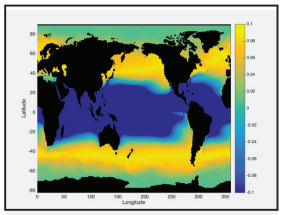

9) Exploration of the Tara Oceans data set to validate our theoretical results

10) Comparison with Phytoplankton diversity from Thomas *et al.* 2012

11) Evolution of phytoplankton thermal niche with an adaptive model using future SST projection from IPCC and a simple thermal traits dynamical model

Choice of the light intensity during the experiments

The experiments were conducted at 100 μmol photons m^{-2} s^{-1} to find an optimal trade-off between non-photolimiting and non-photoinhibiting conditions. As supported by the work of [1], temperature growth response of phytoplankton is weakly coupled with light intensity for moderate light, whereas it could become more dependent to light at higher light intensities for which photoinhibition occurs. [2] showed that marked light-limitation can reduce the optimal growth temperature of phytoplankton by about 5°C. [3] studied the light growth response of *Micromonas* commoda and observed photoinhibition for light intensities higher than 300 μmol photons m^{-2} s^{-1}.
In order to develop a model that accounts for the response to temperature, it was critical to experiment on the potential response, i.e. to assess the maximum growth capacity of strains at each temperature, not to introduce any bias (such as photoinhibition) in the experiments that would have led to an inaccurate estimation of the sole impact of temperature. The intensity of 100 μmol photons m^{-2} s^{-1} was therefore a reasonable trade-off. The BR model being tailored to account for light limitation on growth as well, it would then be possible to describe the coupled limitation of light and temperature, should it appear necessary. However, in the present study, the model proved to accurately compare to in situ data sets with the sole response to temperature, which indicated that additional model complexity through the inclusion of a light response was not necessary

Supplementary Table 1: *Information regarding the Micromonas strains used in the study. The thermal environment at the isolation sites is expressed in °C: yearly averaged temperature ($\bar{T}_S$), minimal temperature (T_S^-), and maximal temperature (T_S^+). The latitude of each isolation site (Lat) is expressed in degree and the growth temperature of cultures (T_{RCC}) is in °C.*

RCC #	Species	Thermotype	T_{RCC} (°C)	$\bar{T}_S$ (°C)	T_S^- (°C)	T_S^+ (°C)	Lat (°)
114	*pusilla*		20	11.48	3.85	20.63	41.5
299	*commoda*	Warm	20	24.89	22.7	27.23	22
451	*commoda*	Warm	20	17.67	10.99	25.34	38.5
497	*pusilla*		20	18.02	13.07	24.2	41.5
746	*bravo*	Cold	15	16.02	13.23	19.31	42.5
829	*bravo*	Warm	20	19.72	14.00	26.73	40.75
834	*pusilla*		20	12.77	9.08	16.73	50.5
1697	*commoda*	Cold	15	10.12	5.76	15.90	59
1862	*bravo*	Cold	15	13.62	9.91	17.58	48.5
2257	*polaris*		4	-0.38	-1.79	3.11	71
2306	*polaris*		4	-0.33	-1.79	3.21	71

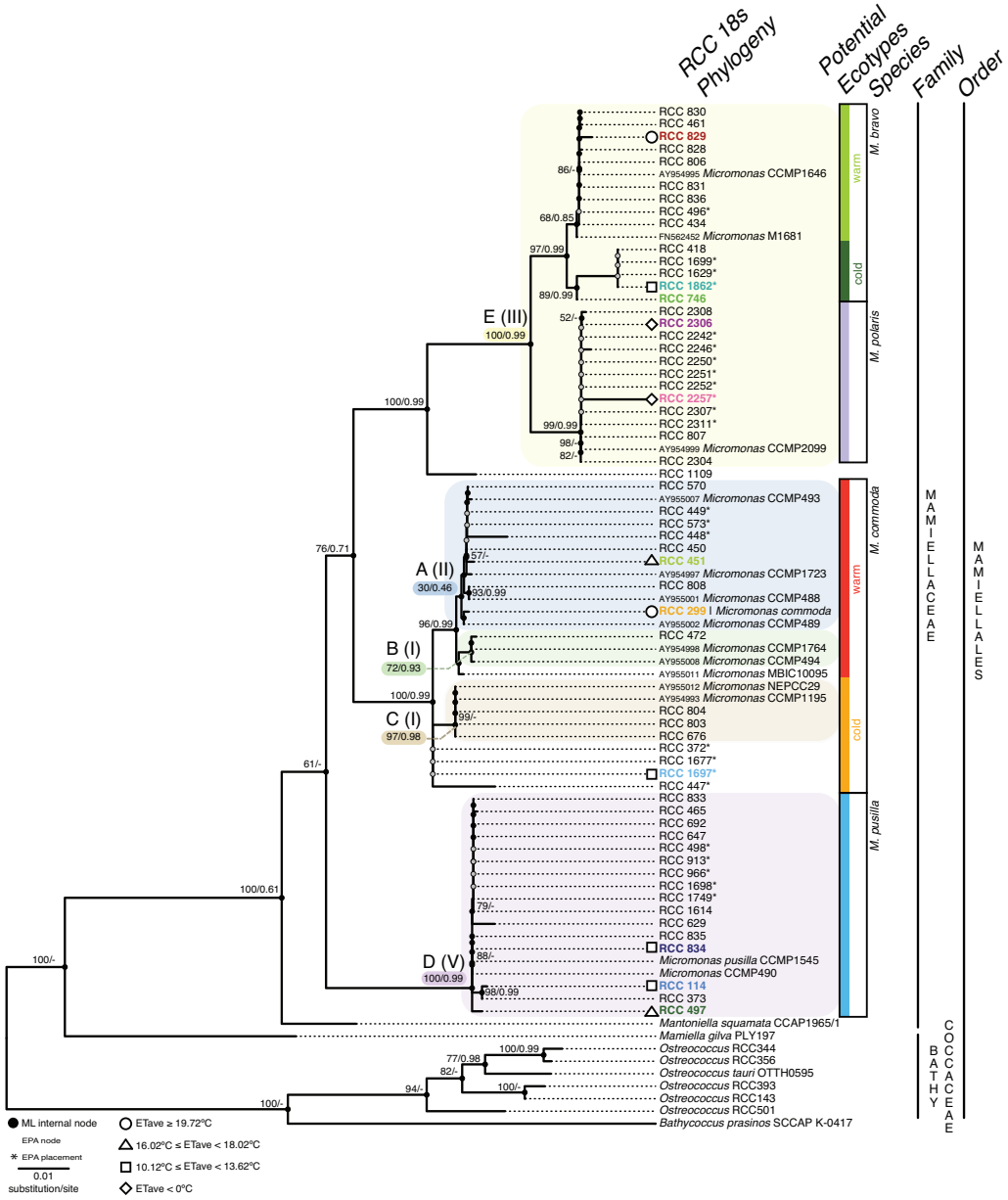

Supplementary Figure 2: *Phylogenetic analysis on 82 18S sequences of RCC strains based on the alignment of [4].*

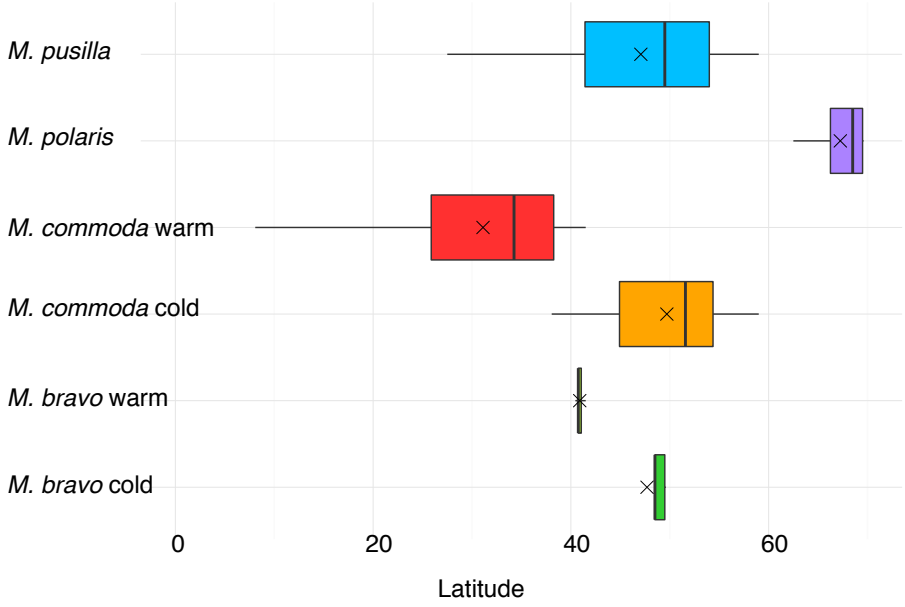

Supplementary Figure 3: *Boxplot of the latitude at which the six phylogenetic groups of Micromonas were isolated*

Supplementary Table 2: *Number of generations during the two-month acclimation calculated with cardinal parameters in Table 6. Symbol "–" indicates a null growth rate.*

RCC #	4°C	7.5°C	9.5°C	12.5°C	20°C	25°C	27.5°C	30°C	32.5°C	35°C
114	–	2.21	6.97	18.37	58.31	71.89	60.06	19.31	–	–
299	–	–	1.08	8.66	53.85	93.38	108.39	111.77	88.39	–
451	–	–	0.03	7.85	57.41	76.56	69.92	46.59	1.84	–
497	6.49	16.62	24.18	37.41	72.39	77.87	58.93	–	–	–
746	–	5.72	15.65	37.37	79.35	–	–	–	–	–
829	1.61	8.56	14.85	26.13	68.02	92.23	94.28	75.91	0.54	–
834	–	1.95	6.47	17.74	60.92	73.60	38.08	–	–	–
1697	12.77	21.22	26.94	36.65	64.63	73.27	–	–	–	–
1862	15.75	27.48	35.38	48.47	81.22	82.49	50.99	–	–	–
2257	35.44	41.36	39.02	24.78	–	–	–	–	–	–
2306	32.42	37.84	35.70	22.67	–	–	–	–	–	–

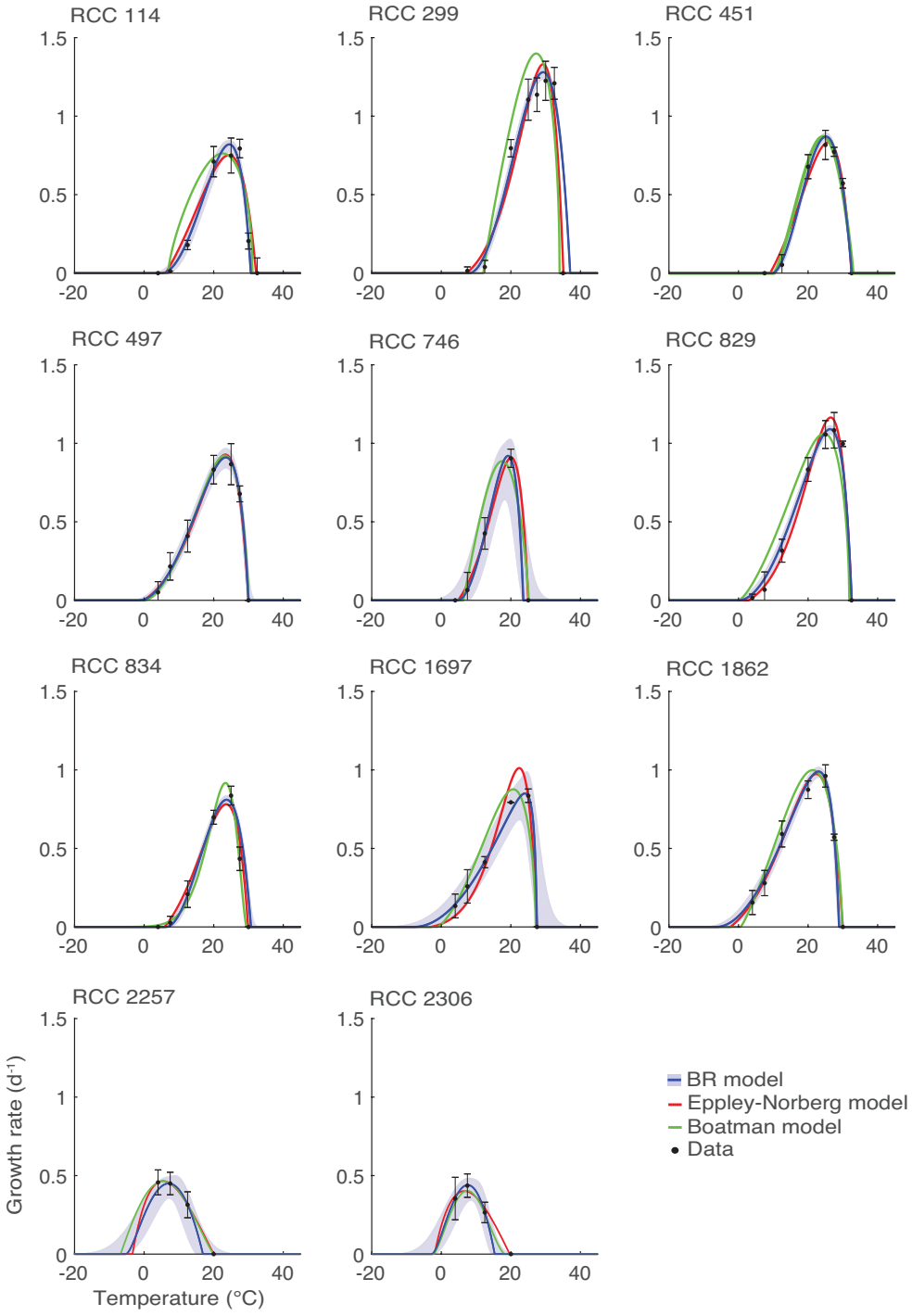

Supplementary Figure 4: *Growth thermal response model fits for the 11 experimental strains. BR model (blue, solid line) with its 95% confidence interval (blue, shaded area), Eppley-Norberg model (red, solid line; [5]), Boatman model (green, solid line, [6]) and average experimental data (black circles) with their standard deviation (n at least = 3).*

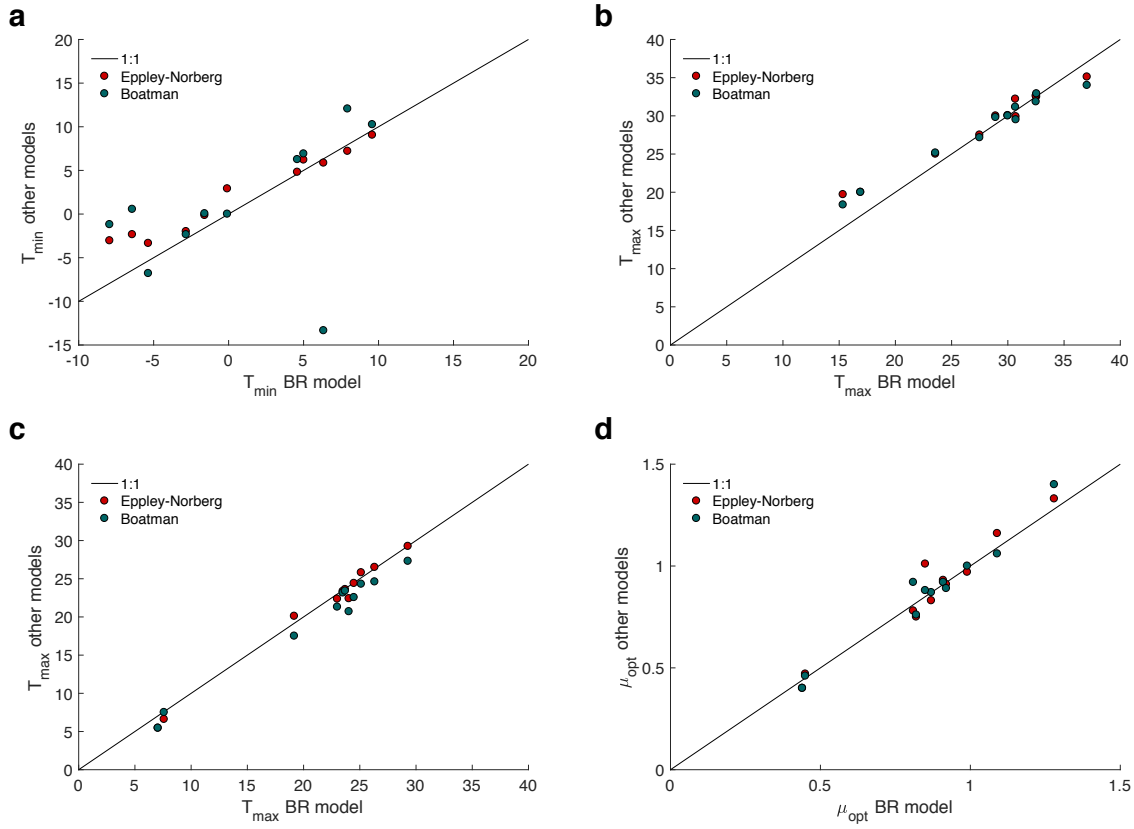

Supplementary Figure 5: *Comparison of cardinal parameters from the three thermal response models tested. (a) T_{min}. (b) T_{max}. (c) T_{opt}. (d) μ_{opt}*

Supplementary Table 3: *Comparison of three models of growth thermal response. AIC is the Akaike Information Criterion calculated as follows: $AIC = 2k - 2ln(MSE)$, with k, the number of parameters to be estimated and MSE, the Mean Square Error calculated with the best fits represented in Supplementary Figure 4. BIC is the Bayesian Information Criterion calculated as follows: $BIC = -2ln(AIC) + kln(n)$, with n, the number of experimental data used for the estimation of the parameters. Minimum values of AIC and BIC represent the best model according to the number of estimated parameters and the quality of the fit.*

Model	Number of parameters	AIC	BIC
BR	4	89.22	178.58
Eppley-Norberg	4	89.35	178.57
Boatman	5	110.51	225.04

Supplementary Table 4: *Parameters of the Eppley-Norberg model [5] for the eleven experimental strains. Parameters were estimated by minimizing the Mean Squared Error (MSE) between model fit and data with the "fminsearch" Matlab function implementing the Nelder-Mead simplex algorithm as described in [7]. The stars in the table indicate that the parameter is explicitly written in the model. The optimal growth rate μ_{opt} is not explicit in the model and is then deduced from the thermal response.*

Strains	T^*_{min}	T^*_{opt}	T^*_{max}	μ_{opt}
114	6.20	24.40	32.20	0.75
299	7.20	29.25	35.10	1.33
451	9.05	25.80	32.50	0.83
497	-0.15	23.35	30.05	0.93
746	4.8	20.10	25.00	0.91
829	2.9	26.50	32.60	1.16
834	5.85	23.60	29.90	0.78
1697	-3.05	22.40	27.50	1.01
1862	-2.35	22.35	30.00	0.97
2257	-3.35	5.45	20.00	0.47
2306	-2.00	6.6	19.7	0.40

Supplementary Table 5: *Parameters of the Boatman model [6] for the eleven experimental strains. Parameters were estimated by minimizing the Mean Squared Error (MSE) between model fit and data with the "fminsearch" Matlab function implementing the Nelder-Mead simplex algorithm as described in [7]. The stars in the table indicate that the parameter is explicitly written in the model. The optimal temperature of growth T_{opt} is not explicit in the model and is then deduced from the thermal response.*

Strains	T^*_{min}	T_{opt}	T^*_{max}	μ^*_{opt}
114	6.90	22.55	31.15	0.76
299	12.05	27.30	34.00	1.40
451	10.25	24.30	32.90	0.87
497	0.05	23.15	30.00	0.92
746	6.25	17.50	25.15	0.89
829	0.00	24.60	31.85	1.06
834	-13.35	23.40	29.50	0.92
1697	-1.20	20.70	27.15	0.88
1862	0.55	21.30	29.80	1.00
2257	-6.80	5.45	20.00	0.46
2306	-2.35	7.50	18.35	0.40

Supplementary Table 6: *Cardinal parameters estimated with the BR model for the eleven strains tested experimentally. Parameters are expressed in °C: minimal temperature of growth (T_{min}), optimal temperature of growth (T_{opt}) and maximal temperature of growth (T_{max}). The optimal growth rate (μ_{opt}) is expressed in day^{-1}. The under and over lines on cardinal parameters represent the lower and upper 95% confidence intervals for each parameter respectively.*

RCC #	$\underline{T_{min}}$	T_{min}	$\overline{T_{min}}$	$\underline{T_{opt}}$	T_{opt}	$\overline{T_{opt}}$	$\underline{T_{max}}$	T_{max}	$\overline{T_{max}}$	$\underline{\mu_{opt}}$	μ_{opt}	$\overline{\mu_{opt}}$
114	1.01	5.01	8.63	22.68	24.49	26.34	30.00	30.68	31.27	0.76	0.82	0.89
299	5.34	7.94	10.32	28.15	29.29	30.56	36.91	37.05	37.14	1.21	1.28	1.35
451	7.53	9.59	11.49	24.49	25.13	25.83	32.44	32.56	32.65	0.82	0.87	0.92
457	-4.36	-1.59	2.54	22.04	23.51	24.42	29.31	30.00	31.94	0.77	0.91	1.00
746	-2.76	4.59	11.16	14.17	19.18	22.18	16.44	23.57	26.26	0.59	0.92	1.06
829	-3.61	-0.08	3.47	25.32	26.33	27.34	32.49	32.51	32.53	1.04	1.09	1.14
834	3.32	6.34	8.86	22.73	23.71	24.69	29.32	30.72	31.90	0.76	0.81	0.87
1697	-16.04	-7.93	2.44	20.38	24.04	25.64	25.50	27.50	35.95	0.73	0.85	1.14
1862	-11.64	-6.42	-1.71	21.87	23.01	24.35	27.59	28.92	29.81	0.94	0.99	1.06
2257	-14.12	-5.35	8.76	4.35	7.03	11.13	8.04	16.91	22.50	0.35	0.45	0.54
2306	-9.74	-2.83	7.58	4.68	7.60	12.03	11.00	15.35	18.37	0.31	0.44	0.53

Supplementary Table 7: *Parameters of of the Eppley model [8] for the 6 thermotypes. The Eppley model equation is: $\mu_{opt} = a.e^{b.T_{opt}}$.The parameters a and b are obtained from the best fit between μ_{opt} and T_{opt} considering all strains within each thermotype.*

Thermotype	a	b
M.commoda Cold	0.39	0.04
M.commoda Warm	0.2	0.06
M.polaris	0.34	0.03
M.bravo Cold	0.28	0.05
M.bravo Warm	0.88	0.007
M.pusilla	0.39	0.04

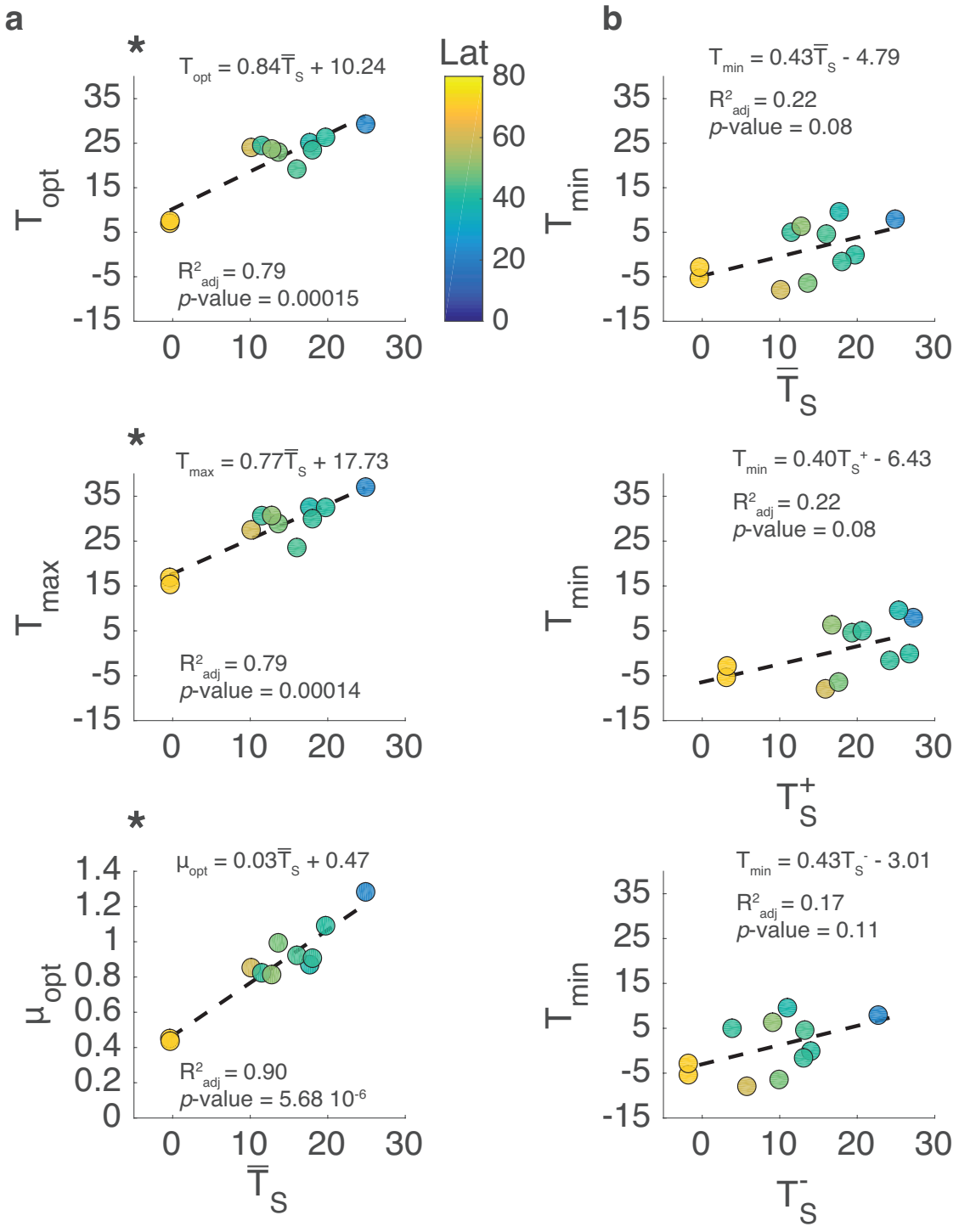

Supplementary Figure 6: *Linear relationships between cardinal parameters and environmental parameters for the eleven strains tested experimentally. a) Relationships between T_{opt}, T_{max} and μ_{opt} vs. the average surface temperature at the isolation site $\bar{T}_S$. b) Relationships between T_{min} vs. averaged surface temperature at the isolation site $\bar{T}_S$, maximal surface temperature at the isolation site T_S^+ and minimal surface temperature at the isolation site T_S^-. Latitude at the isolation site is expressed with the color-bar. The star on top of the vertical axis represents a statistical significant relationship (p-value < 0.05).*

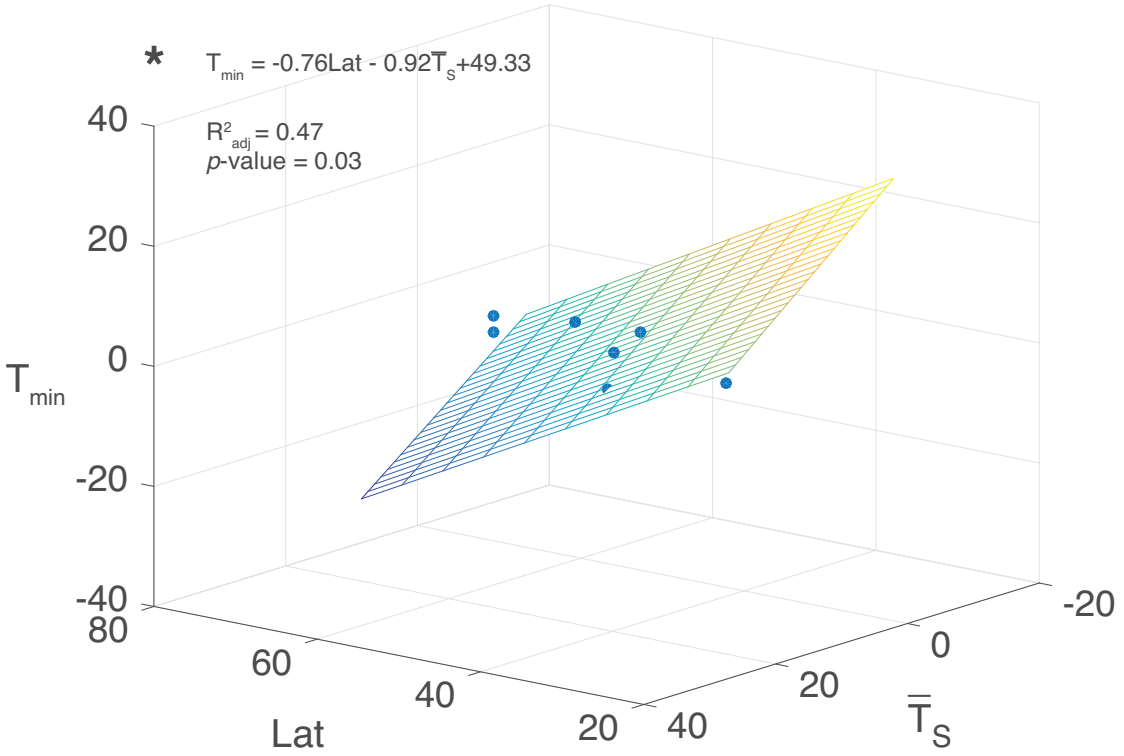

Supplementary Figure 7: *Linear relationships between T_{min} vs. the latitude at the isolation site Lat and the average surface temperature at the isolation site $\bar{T}_S$ for the eleven strains tested experimentally. The star on top of the vertical axis represents a statistical significant relationship (p-value < 0.05).*

Supplementary Table 8: *Cardinal parameters (in °C), optimal growth rate (in day^{-1}) and thermal niche width (in °C) of the six thermotypes with their associated standard deviation.*

Thermotypes	T_{min}	T_{opt}	T_{max}	μ_{opt}	Thermal niche
M. commoda cold	0.15 ± 5.06	20.11 ± 1.38	26.84 ± 1.30	0.78 ± 0.04	26.69
M. commoda warm	4.53 ± 5.15	27.96 ± 1.42	34.39 ± 1.34	1.10 ± 0.10	29.86
M. polaris	-4.53 ± 1.38	10.55 ± 1.76	18.21 ± 1.66	0.45 ± 0.03	22.74
M. bravo cold	-0.11 ± 1.15	20.67 ± 0.71	27.40 ± 0.67	0.88 ± 0.03	27.51
M. bravo warm	-0.24 ± 1.13	27.03 ± 0.78	33.41 ± 0.74	1.05 ± 0.005	33.65
M. pusilla	-0.11 ± 4.84	21.22 ± 3.01	29.46 ± 2.84	0.78 ± 0.11	29.57

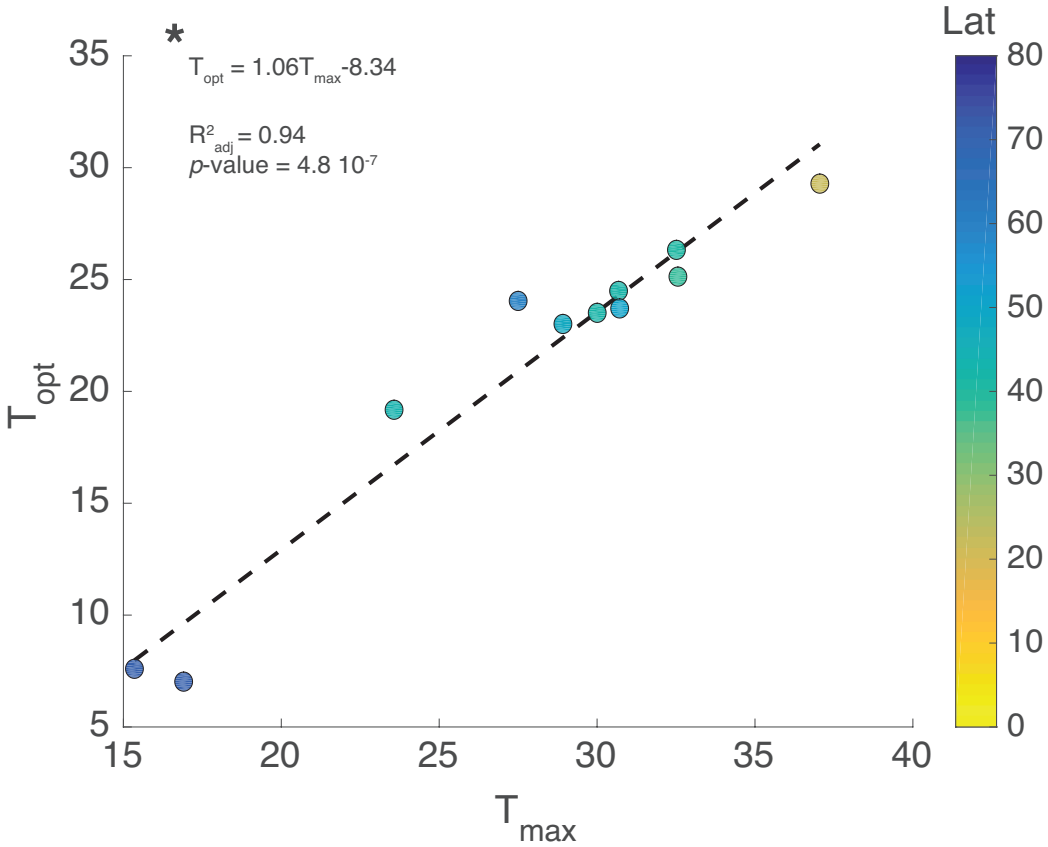

Supplementary Figure 8: *Linear relationship between the maximal temperature of growth (T_{max}) and the optimal temperature of growth (T_{opt}) for the eleven strains tested experimentally. The star on top of the vertical axis represents a statistically significant relationship (p-value < 0.05).*

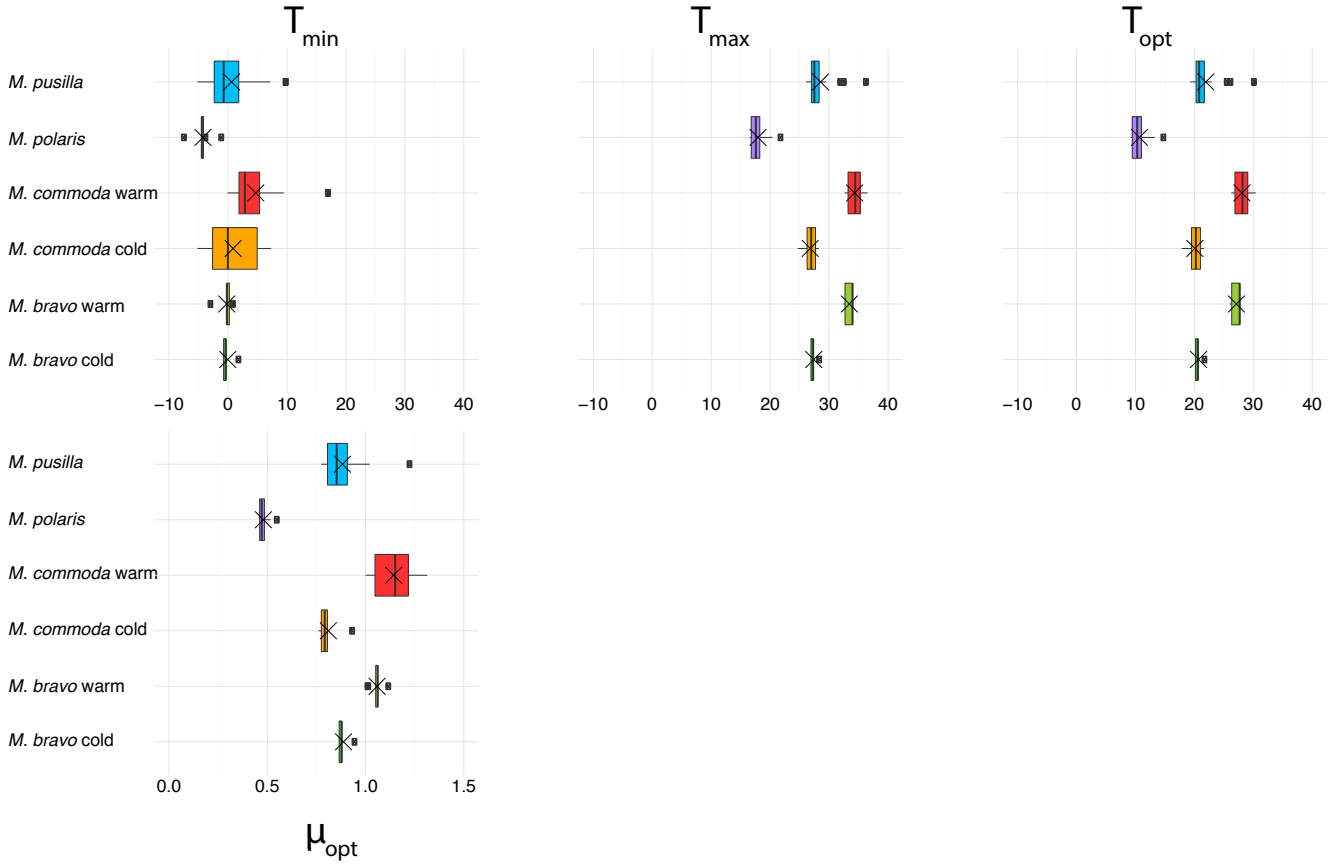

Supplementary Figure 9: *Boxplot of cardinal parameters (T_{min}, T_{max} and T_{opt}) and optimal growth rate (μ_{opt}) for the 6 Micromonas thermotypes.*

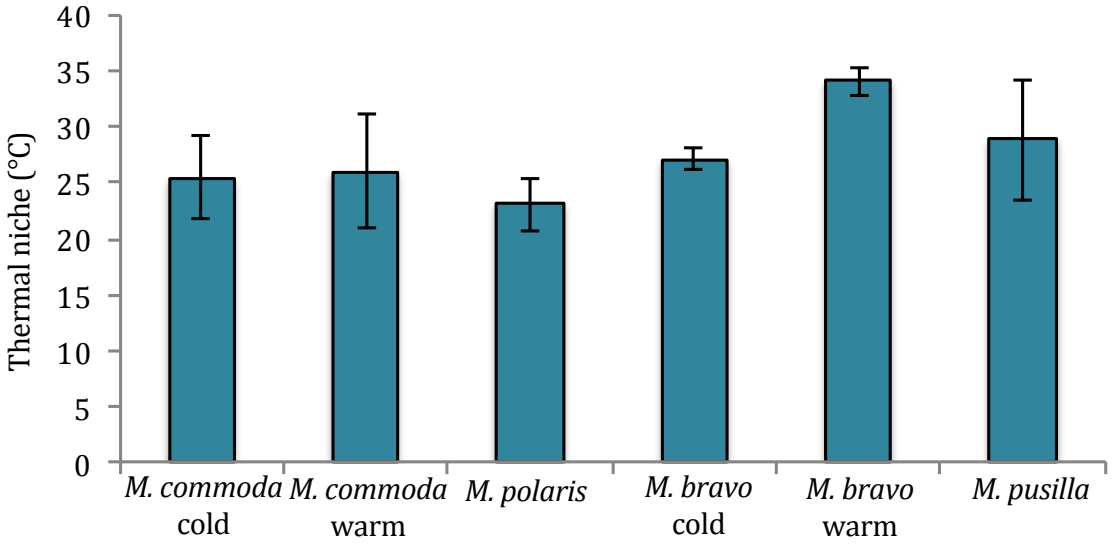

Supplementary Figure 10: *Thermal niche width ($T_{max} - T_{min}$) for the six Micromonas thermotypes. Error bars represent the standard deviation.*

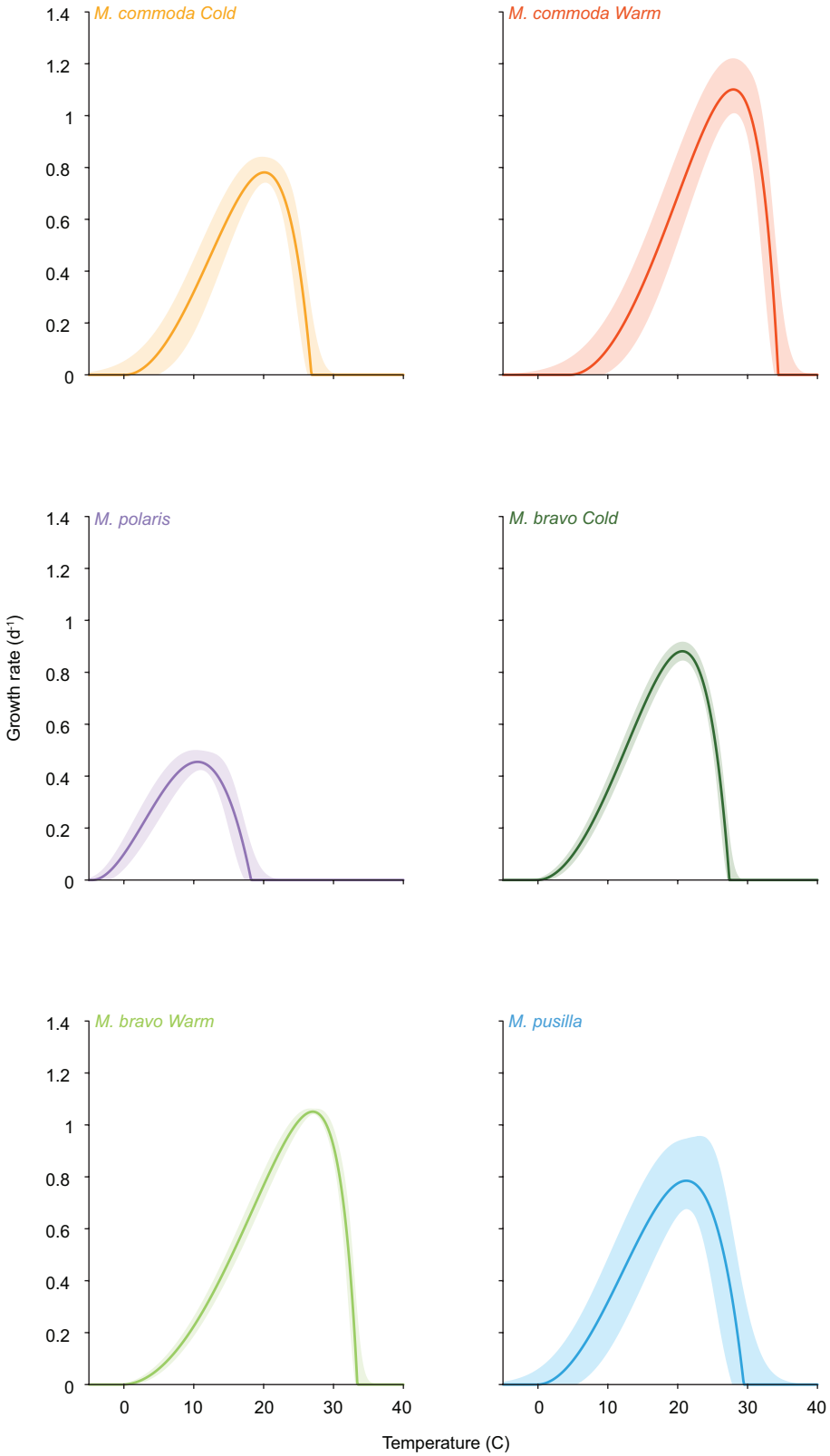

Supplementary Figure 11: *Average thermal response of the six Micromonas thermotypes (solid lines) within their associated 95% confidence interval (shaded area).*

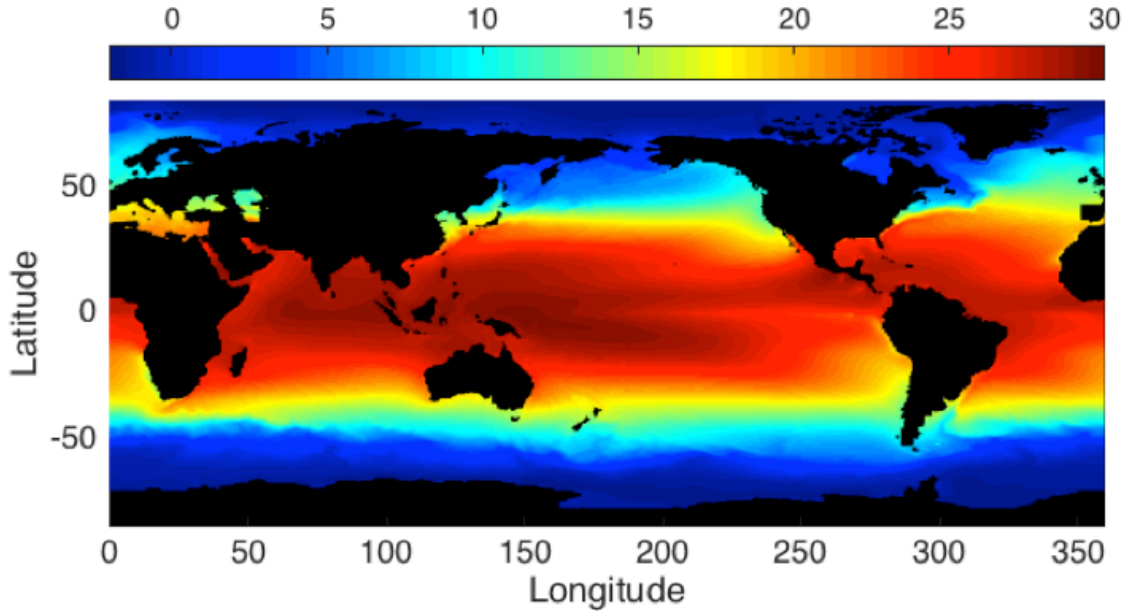

Supplementary Figure 12: *Annual average SST (°C) from the Copernicus Marine Service Monitoring for the period 2005 to 2014.*

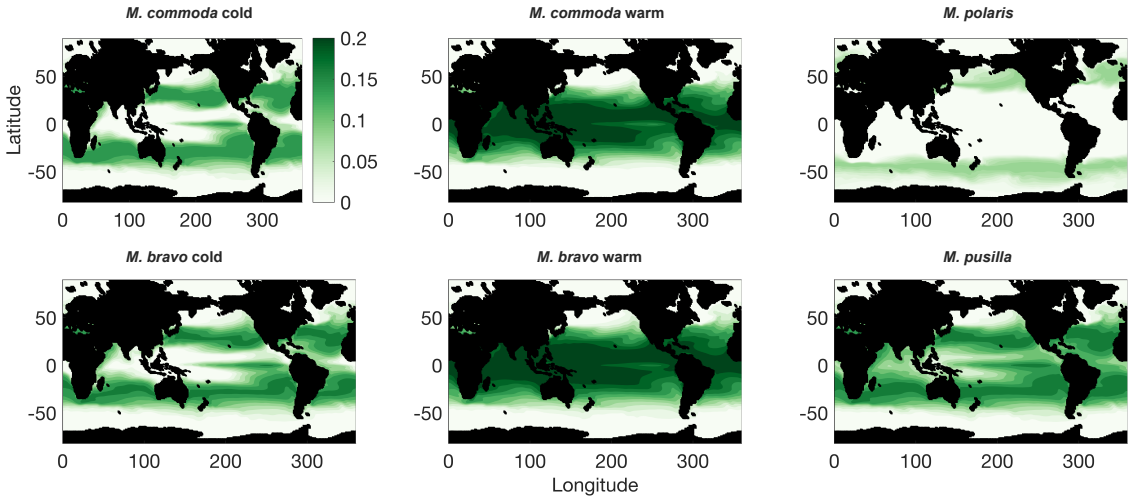

Supplementary Figure 13: *Average distribution of the six Micromonas thermotypes over the period 2005-2014. The color-bar represents the distribution index* $D_i = \frac{\mu_i(T)}{\sum \mu_{opt,i}}$ *depending on the global SST from the Copernicus Marine Service Monitoring.*

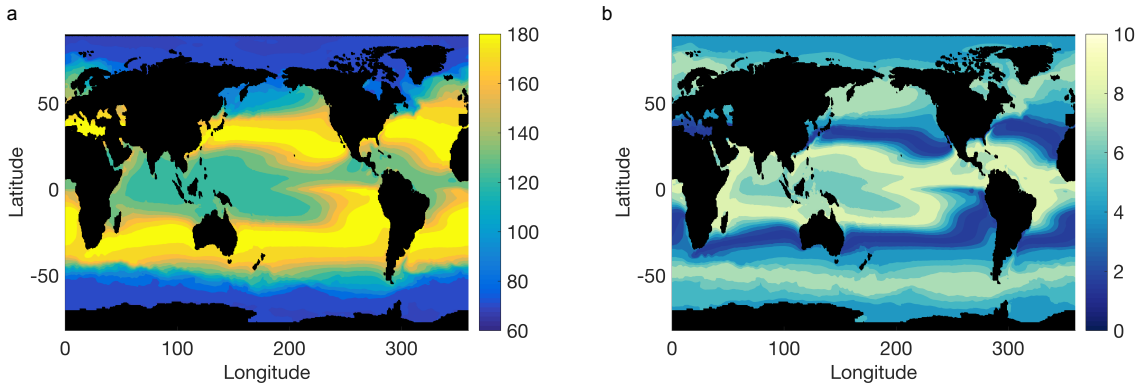

Supplementary Figure 14: *Statistics of the Micromonas diversity calculated according to 10,000 set of parameters for the 6 thermotypes. (a) Global average diversity. (b) Standard error of the mean expressed as the % difference with the average diversity.*

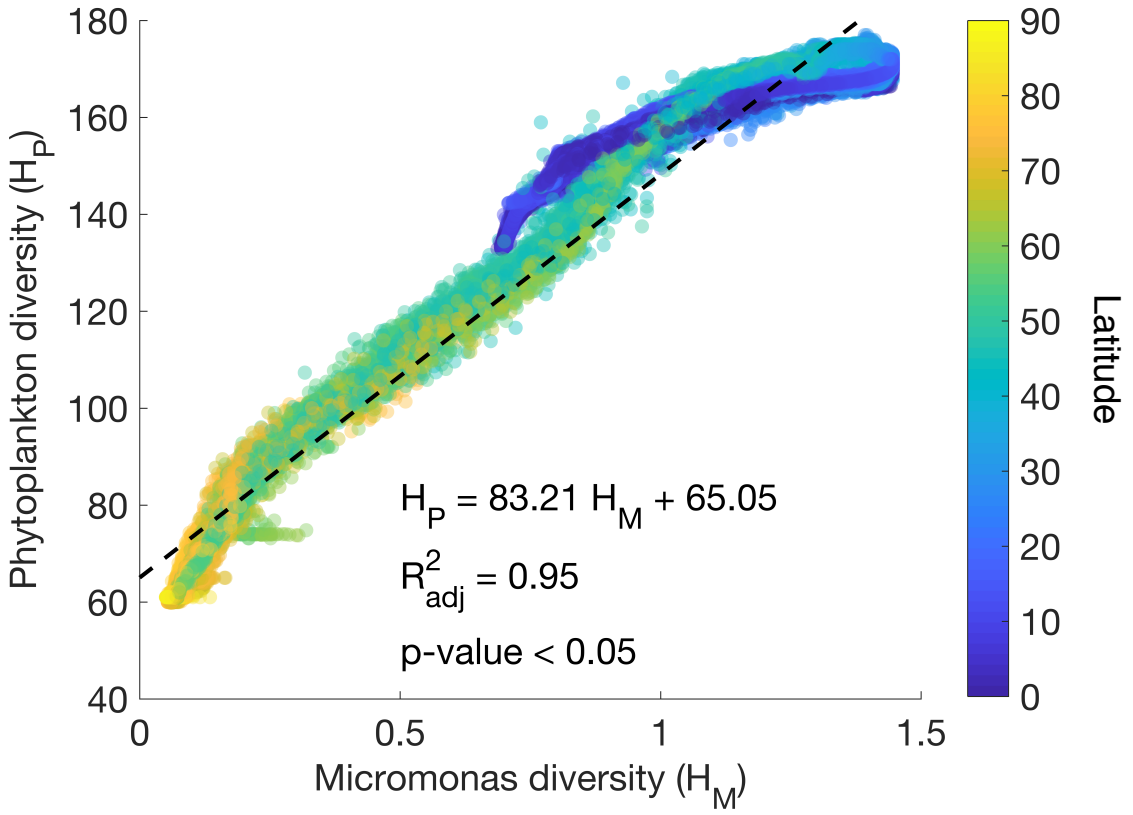

Supplementary Figure 15: *Linear relationships between phytoplankton diversity (H_T - [9]) and Micromonas interspecific diversity (H_M - present study).*

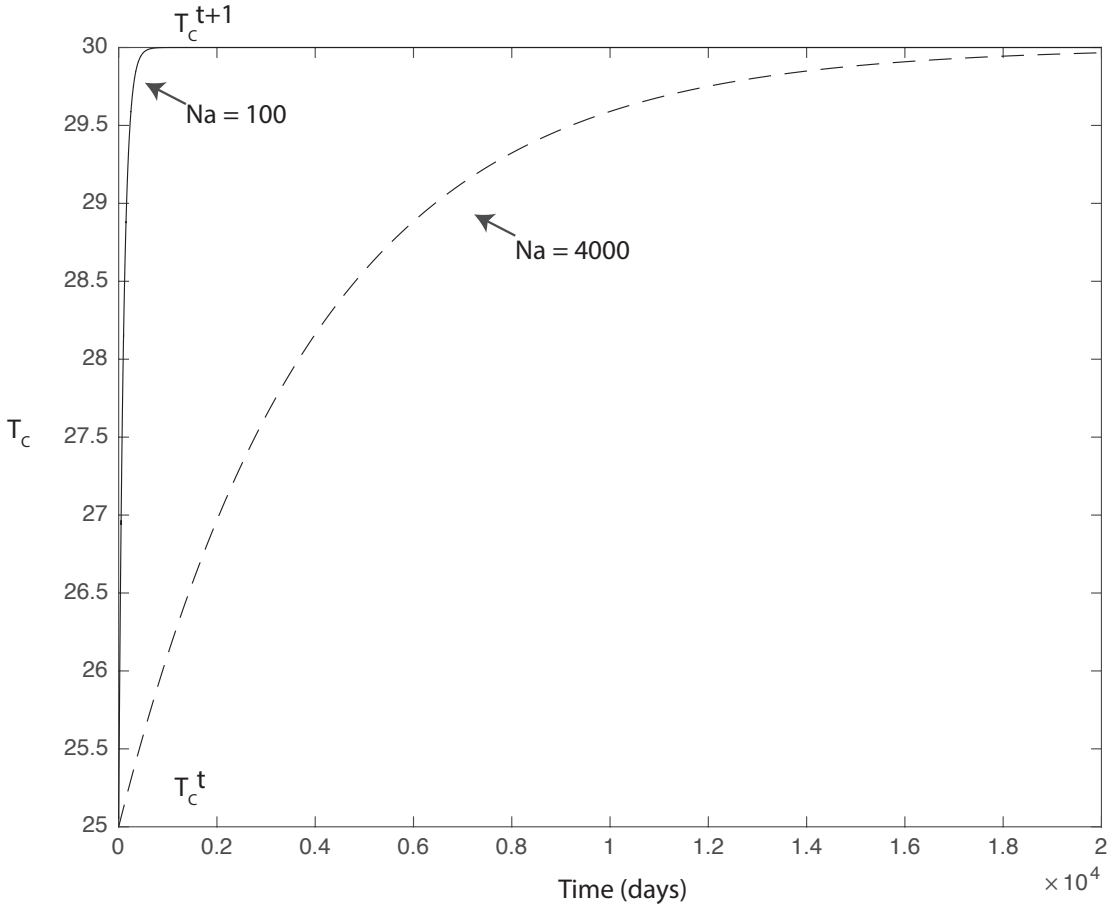

Supplementary Figure 16: *Example of evolution of cardinal parameters with the dynamical model (eq. 2 in the main manuscript). Here we presented the generic cardinal parameter T_C (T_{min}, T_{opt}, T_{max}) between time t (T_C^t) and time $t+1$ (T_C^{t+1}) for two evolution time scales: fast ($Na = 100$ generations) and slow ($Na = 4000$ generation).*

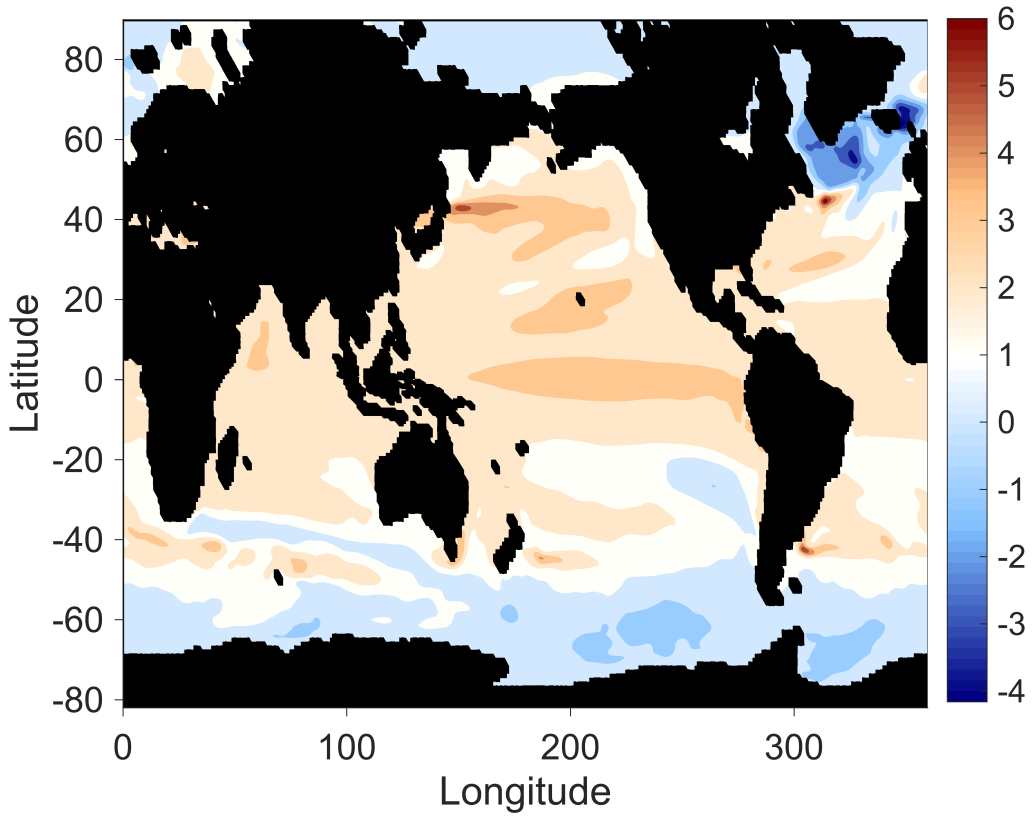

Supplementary Figure 17: *SST anomalies between the present (2001-2010) and future (2091-2100) periods. Projections of global future temperature regimes were obtained from the NOAA GFDL CM2.1 [10, 11] driven with the SRES A2 emissions scenario [12].*

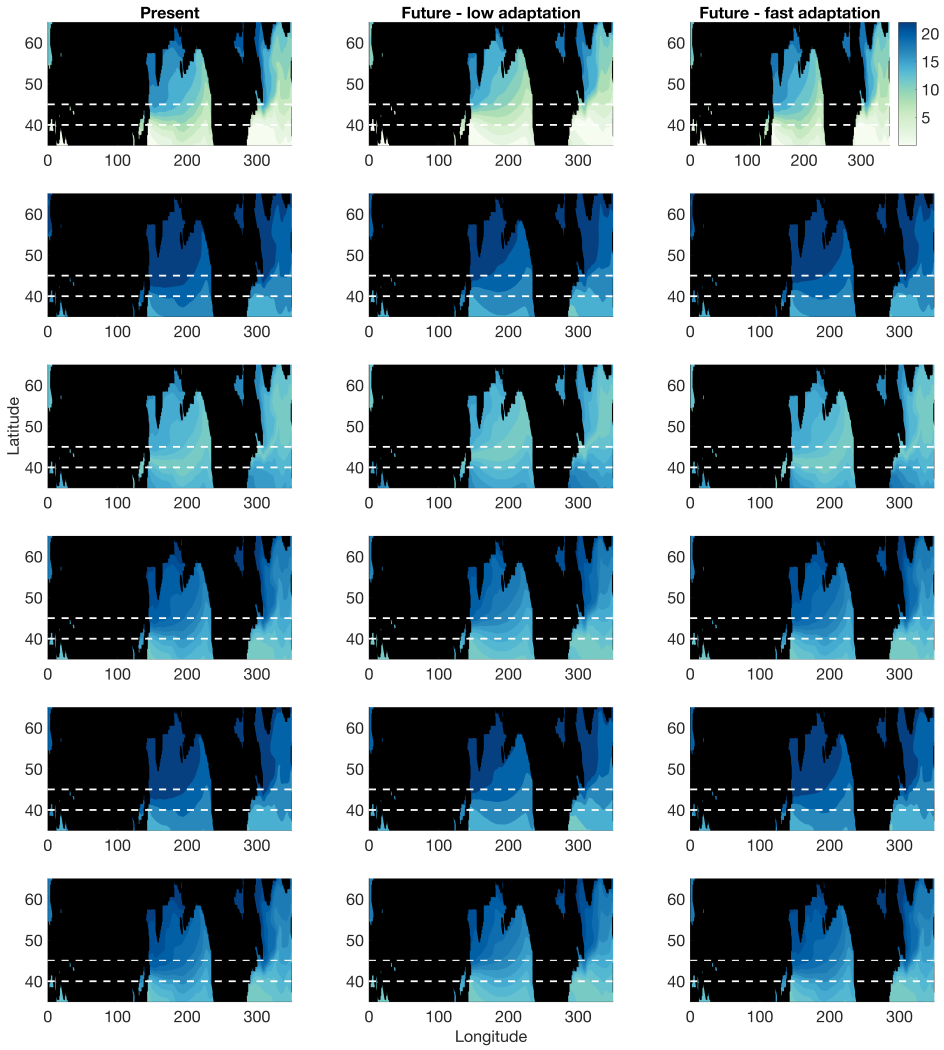

Supplementary Figure 18: *Comparison of the index* $\mid T_{opt} - \overline{T_S} \mid$ *for the hypothesis Specialist-generalist with constant thermal niche for slow and fast adaptation scenarios. Low values indicate that* T_{opt} *is close to* $\overline{T_S}$*. The maps are centered on the 35-65°N. White dashed lines represent the 40-45°N zone where we observed a diversity gain related to an increase in temperature in the future.*

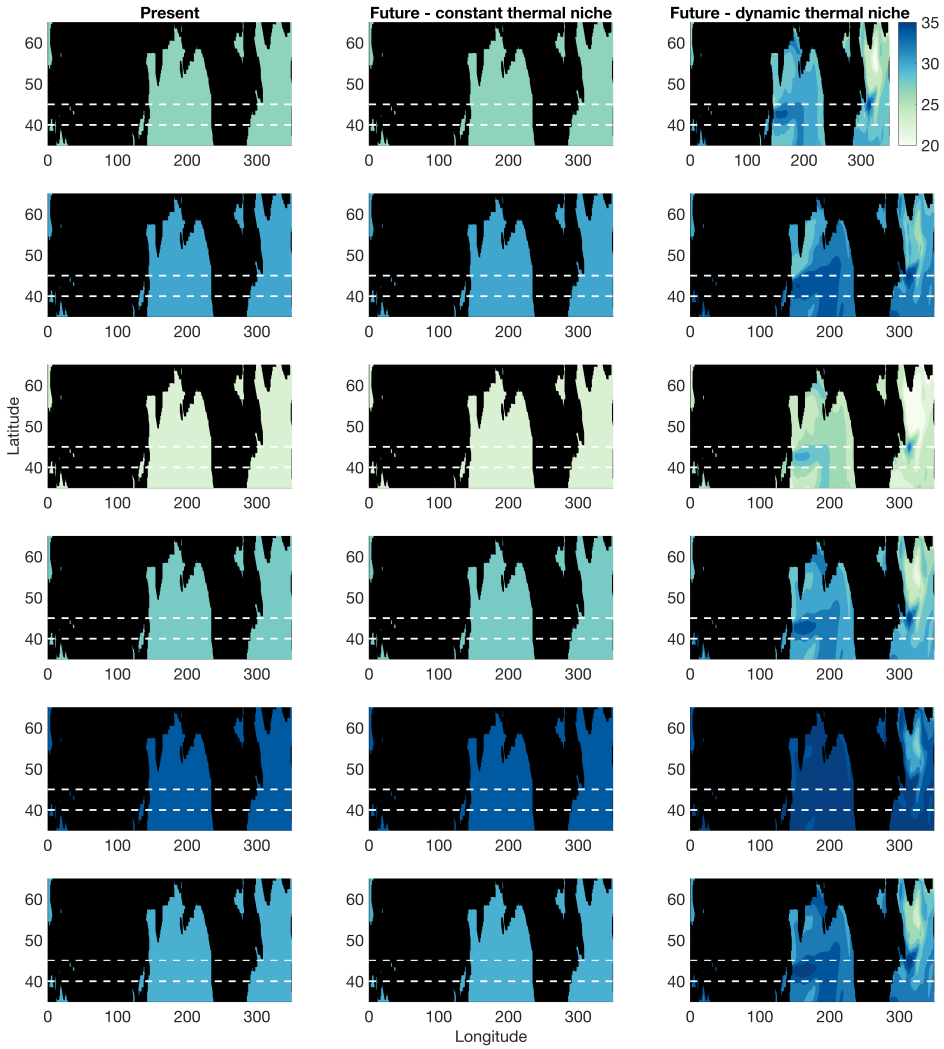

Supplementary Figure 19: *Comparison of the thermal niche ($T_{max} - T_{min}$) for the fast scenario ($Na = 100$) for two hypotheses: Specialist-generalist with constant thermal niche and with dynamic thermal niche. The maps are centered on the 35-65°N. White dashed lines represent the 40-45°N zone where we observed a diversity gain related to an increase in temperature in the future.*

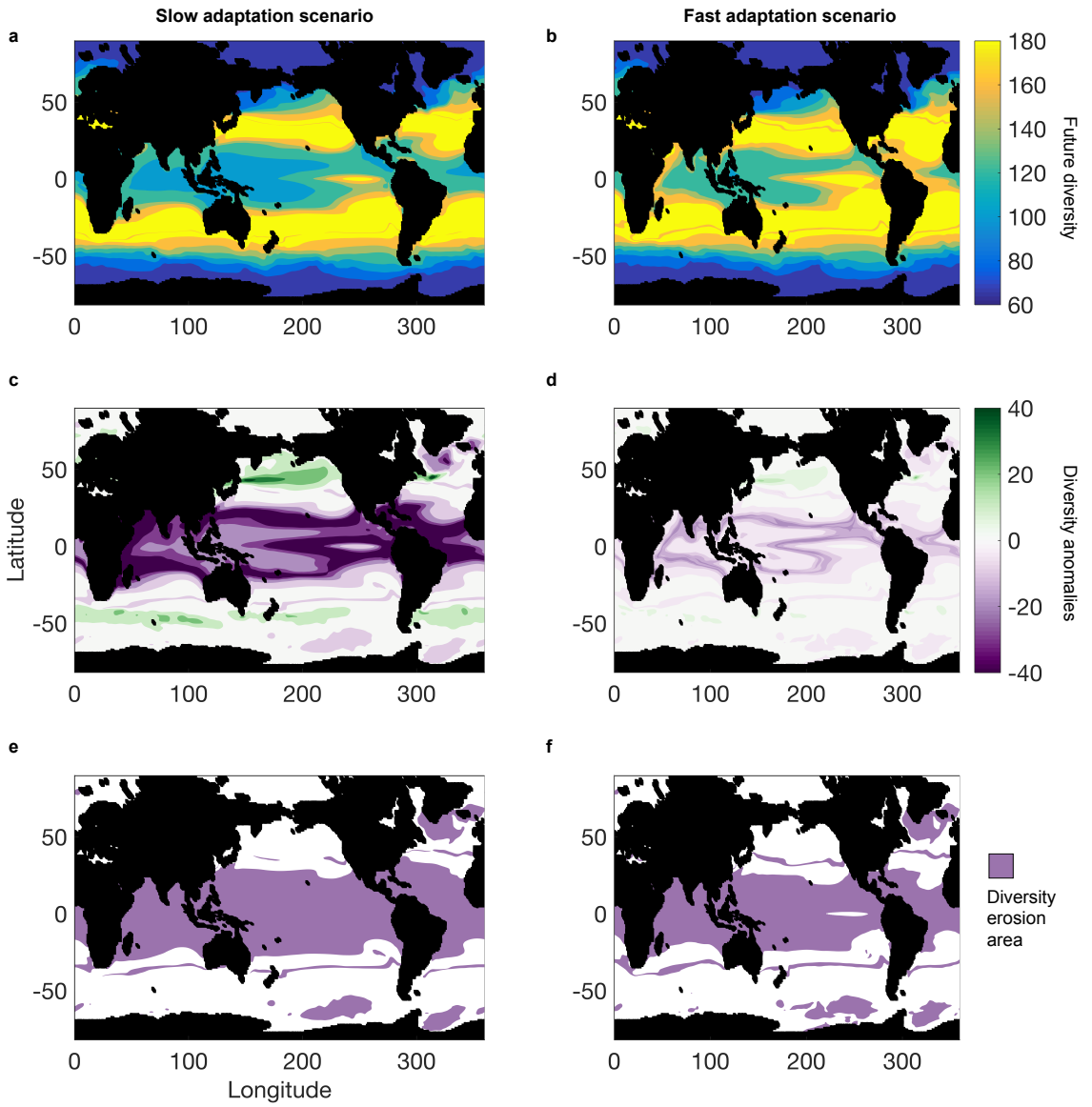

Supplementary Figure 20: *Evolution of diversity for two different scenarios of adaptation kinetic (a,c,e. $Na = 100$ and b,d,f. $Na = 10^6$) between the present (2001-2010) and the future (2091-2100) periods with the Specialist-generalist hypothesis with constant thermal niche. (a-b) Future diversity. (c-d) Diversity anomalies calculated as the difference between future and present diversity. (e-f) Diversity erosion area represent the area where the anomalies are negatives.*

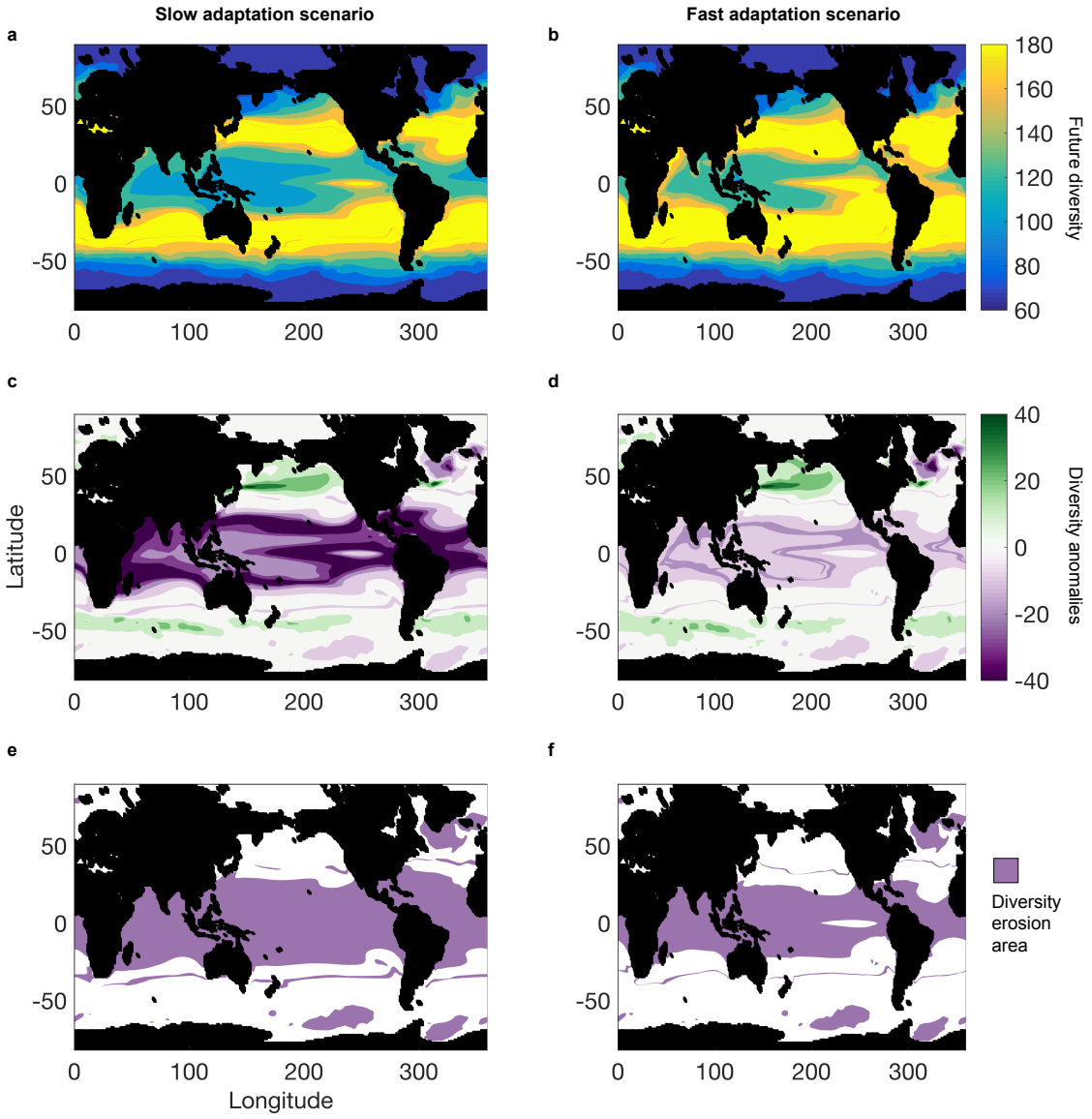

Supplementary Figure 21: *Evolution of diversity for two different scenarios of adaptation kinetic (a,c,e. $Na = 100$ and b,d,f. $Na = 10^6$) between the present (2001-2010) and the future (2091-2100) periods with the Specialist-generalist hypothesis with dynamic thermal niche. (a-b) Future diversity. (c-d) Diversity anomalies calculated as the difference between future and present diversity. (e-f) Diversity erosion area represent the area where the anomalies are negatives.*

References

[1] Bernard O, and Rémond B. 2012. Validation of a simple model accounting for light and temperature effect on microalgal growth. Bioresource technology 123: 520–527.

[2] Edwards KF, Thomas MK, Klausmeier CA, and Litchman E. 2016. Phytoplankton growth and the interaction of light and temperature: A synthesis at the species and community level. Limnology and Oceanography 61: 1232–1244.

[3] Cuvelier ML, Guo J, Ortiz AC, Van Baren MJ, Tariq MA, Partensky F, and Worden AZ. 2017. Responses of the picoprasinophyte *Micromonas commoda* to light and ultraviolet stress. PloS one 12: e172135.

[4] Marin B, and Melkonian M. 2010. Molecular phylogeny and classification of the Mamiellophyceae class. nov. (Chlorophyta) based on sequence comparisons of the nuclear- and plastid-encoded rRNA operons. Protist 161: 304–336.

[5] Norberg J. 2004. Biodiversity and ecosystem functioning: a complex adaptive systems approach. Limnology and Oceanography 49: 1269–1277.

[6] Boatman TG, Lawson T, and Geider RJ. 2017. A key marine diazotroph in a changing ocean: The interacting effects of temperature, CO2 and light on the growth of *Trichodesmium erythraeum* IMS101. PloS one 12: e0168796.

[7] Lagarias JC, Reeds JA, Wright MH, and Wright PE. 1998. Convergence properties of the nelder-mead simplex method in low dimensions. SIAM Journal on optimization 9: 112–147.

[8] Eppley RW. 1972. Temperature and phytoplankton growth in the sea. Fishery Bulletin 70: 1063–1085.

[9] Thomas MK, Kremer CT, Klausmeier CA, and Litchman E. 2012. A Global Pattern of Thermal Adaptation in Marine Phytoplankton. Science 338: 1085–1088.

[10] Griffies SM, Gnanadesikan AWDK, Dixon KW, Dunne JP, Gerdes R, Harrison MJ, *et al.* 2005. Formulation of an ocean model for global climate simulations. Ocean Science 1: 45–79.

[11] Delworth T, Broccoli AJ, Rosati A, Stouffer RJ, Balaji V, Beesley JA, *et al.* 2006. GFDL's CM2 global coupled climate models. Part I: Formulation and simulation characteristics. Journal of Climate 19: 643–674.

[12] Nakicenovic N, Alcamo J, Grubler A, Riahi K, Roehrl RA, Rogner HH, and Victor N. 2000. Special report on emissions scenarios: A special report of Working Group III of the Intergovernmental Panel on Climate Change. Nakicenovic N, Swart R, Eds. (Cambridge University Press, Cambridge, UK; Working Group III of the Intergovernmental Panel on Climate Change.

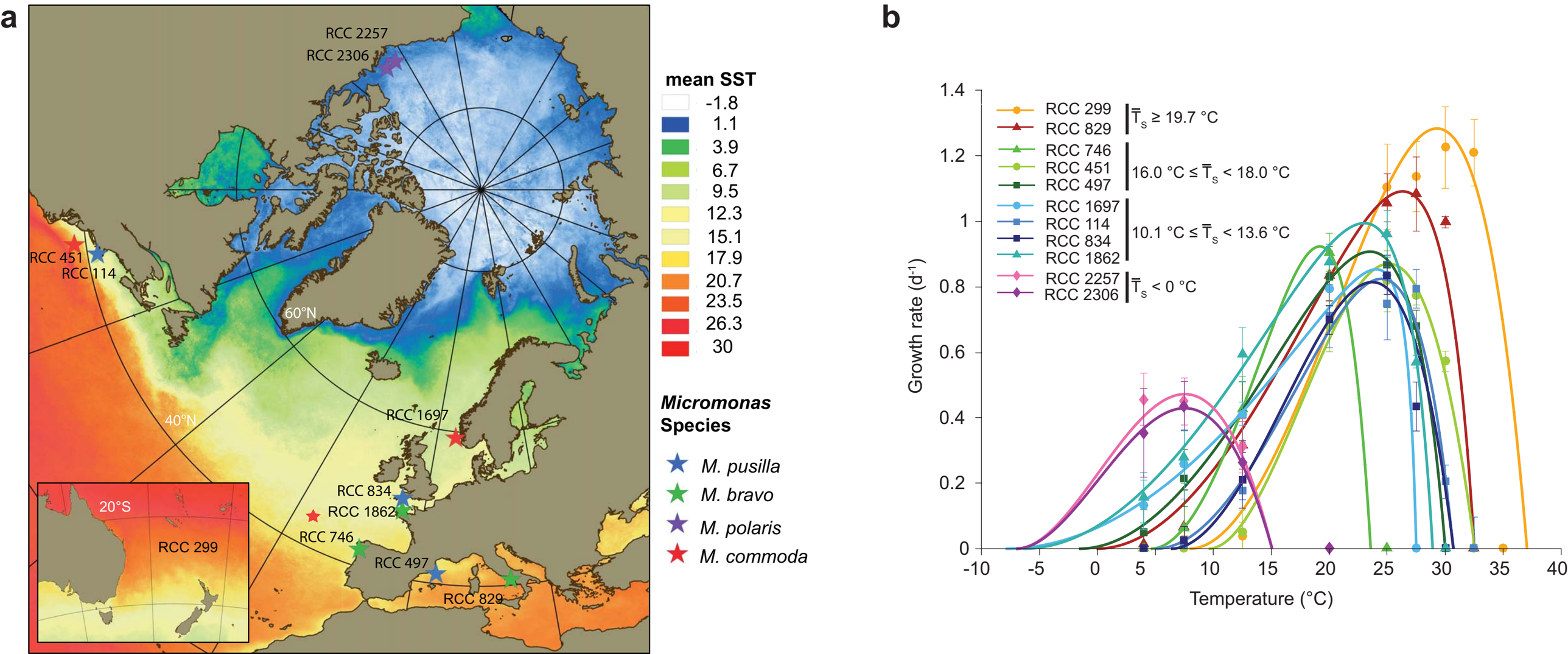
a
RCC 2257
RCC 2306
RCC 451
RCC 114
60°N
40°N
RCC 1697
RCC 834
RCC 1862
RCC 746
RCC 497
RCC 829
20°S
RCC 299
mean SST
-1.8
1.1
3.9
6.7
9.5
12.3
15.1
17.9
20.7
23.5
26.3
30
Micromonas Species
M. pusilla
M. bravo
M. polaris
M. commoda
b
RCC 299
RCC 829
$\bar{T}_S \geq 19.7$ °C
RCC 746
RCC 451
RCC 497
16.0 °C ≤ $\bar{T}_S$ < 18.0 °C
RCC 1697
RCC 114
RCC 834
RCC 1862
10.1 °C ≤ $\bar{T}_S$ < 13.6 °C
RCC 2257
RCC 2306
$\bar{T}_S$ < 0 °C
Growth rate (d-1)
Temperature (°C)
1.4
1.2
1
0.8
0.6
0.4
0.2
0
-10
-5
0
5
10
15
20
25
30
35
40

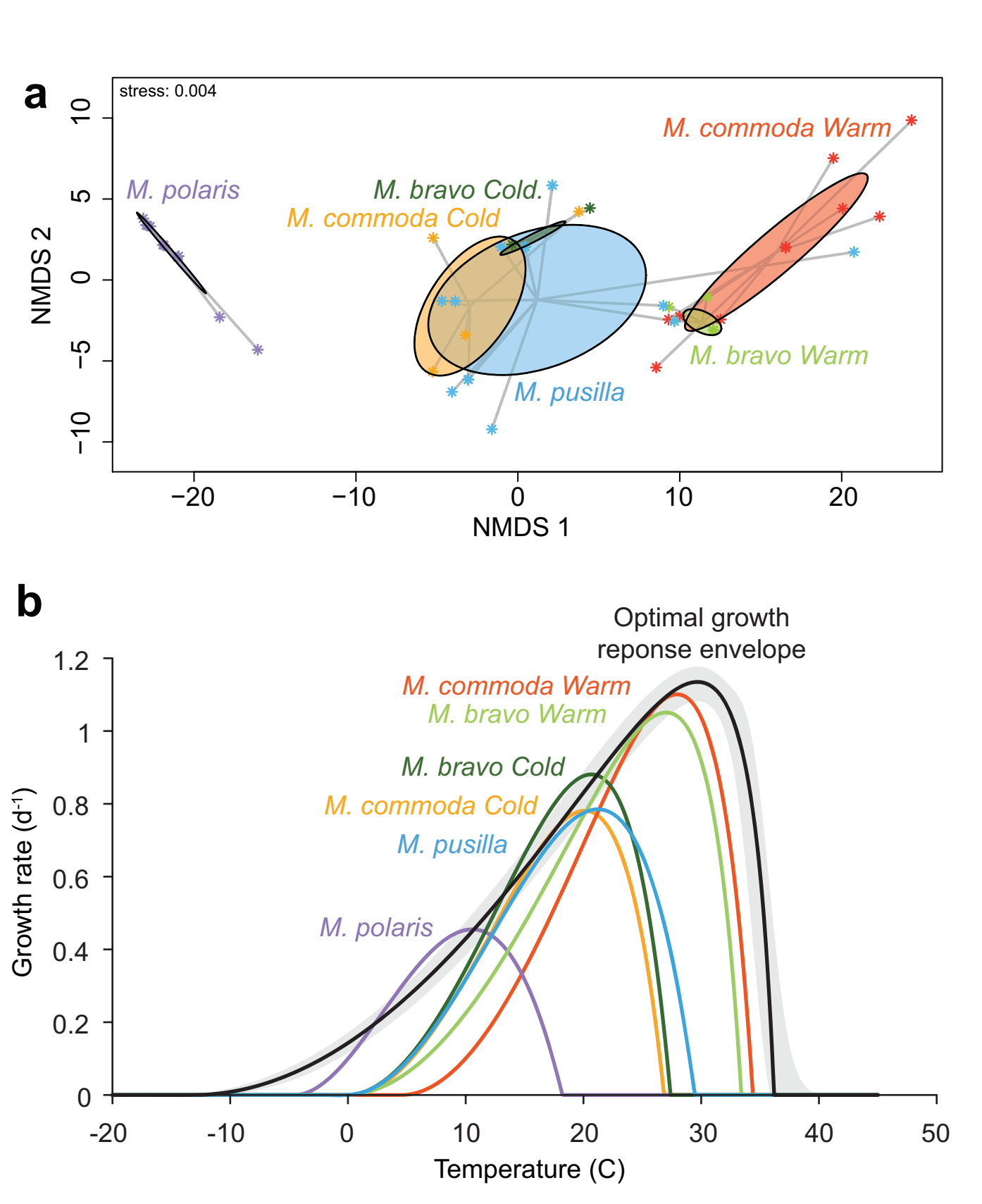
a
stress: 0.004
M. commoda Warm
M. polaris
M. bravo Cold.
M. commoda Cold
M. bravo Warm
M. pusilla
NMDS 2
NMDS 1
10
5
0
−5
−10
−20
−10
0
10
20
b
Optimal growth
reponse envelope
M. commoda Warm
M. bravo Warm
M. bravo Cold
M. commoda Cold
M. pusilla
M. polaris
Growth rate (d-1)
Temperature (C)
1.2
1
0.8
0.6
0.4
0.2
0
-20
-10
0
10
20
30
40
50

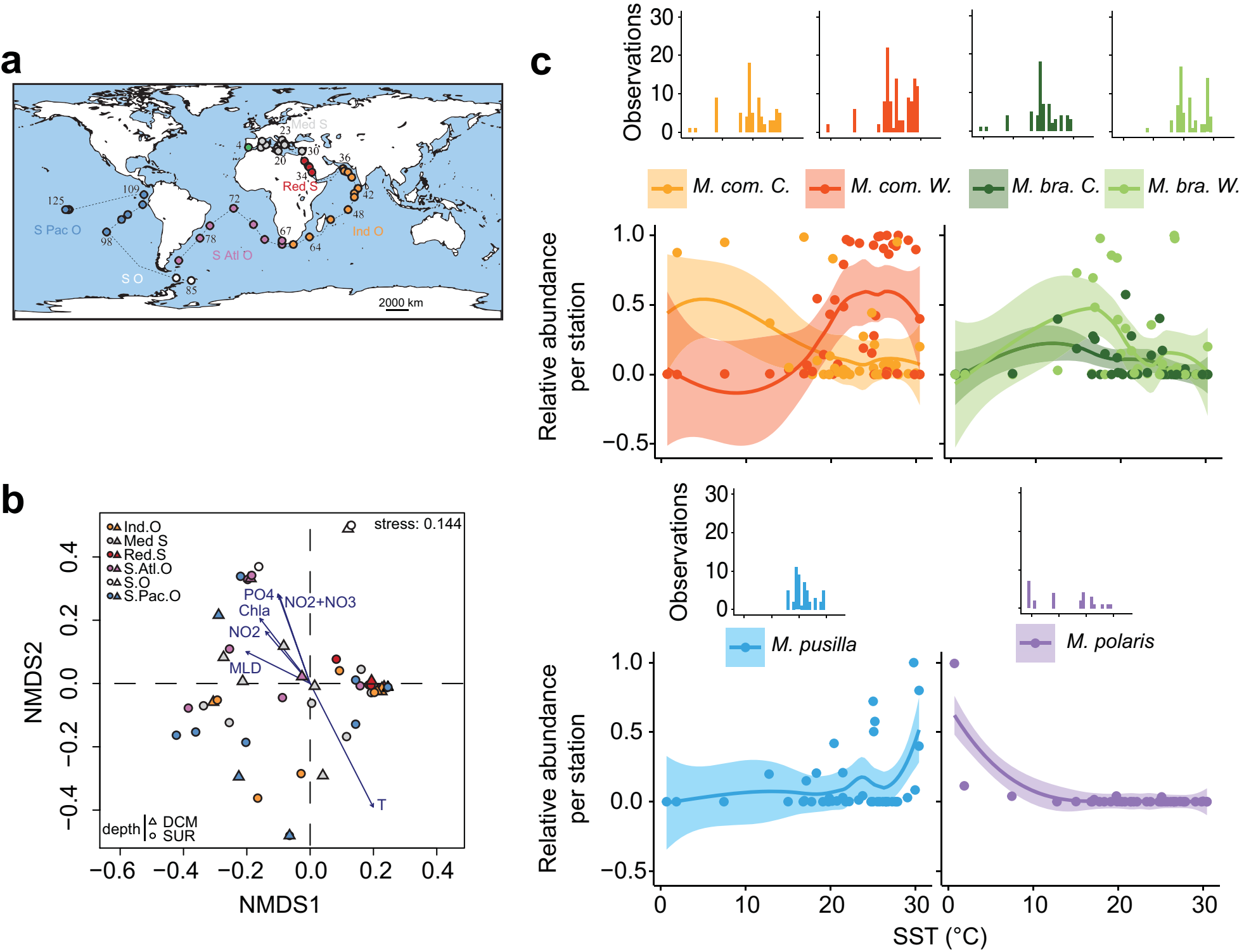
a
Med S
Red S
Ind O
S Atl O
S Pac O
S O
2000 km
b
Ind.O
Med S
Red.S
S.Atl.O
S.O
S.Pac.O
stress: 0.144
PO4
NO2+NO3
Chla
NO2
MLD
T
depth DCM SUR
NMDS1
NMDS2
c
Observations
M. com. C.
M. com. W.
M. bra. C.
M. bra. W.
Relative abundance per station
M. pusilla
M. polaris
SST (°C)

a

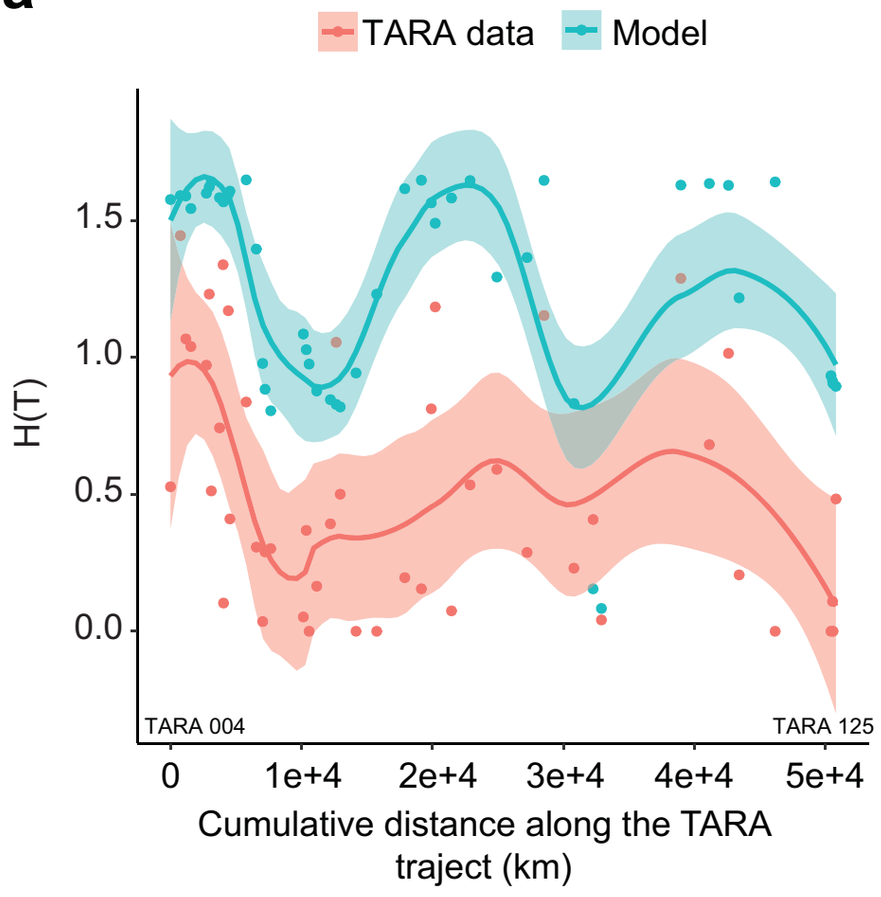
TARA data
Model
H(T)
1.5
1.0
0.5
0.0
TARA 004
TARA 125
0
1e+4
2e+4
3e+4
4e+4
5e+4
Cumulative distance along the TARA traject (km)

b

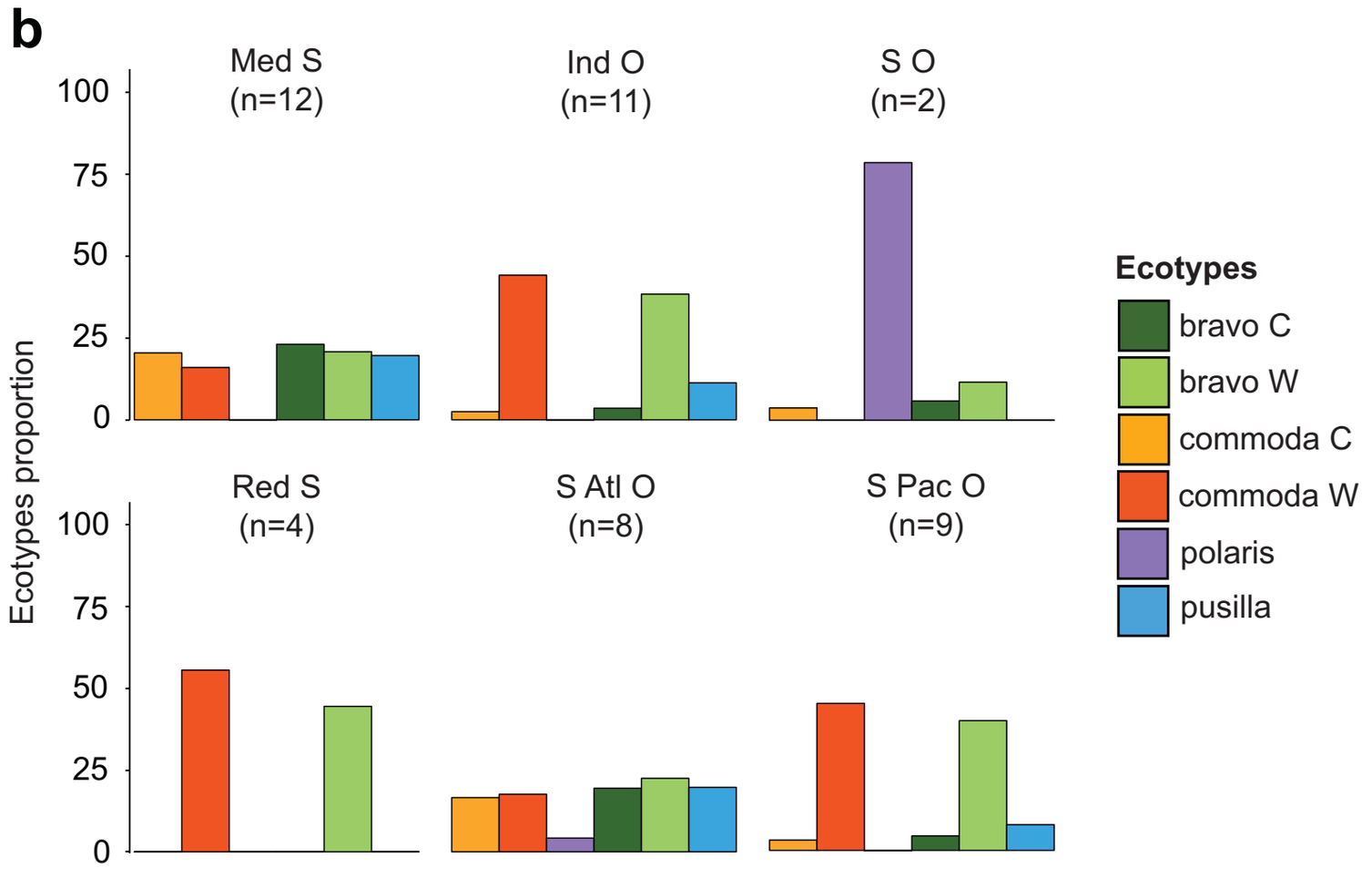
Med S (n=12)
Ind O (n=11)
S O (n=2)
Red S (n=4)
S Atl O (n=8)
S Pac O (n=9)
Ecotypes proportion
100
75
50
25
0
Ecotypes
bravo C
bravo W
commoda C
commoda W
polaris
pusilla

c

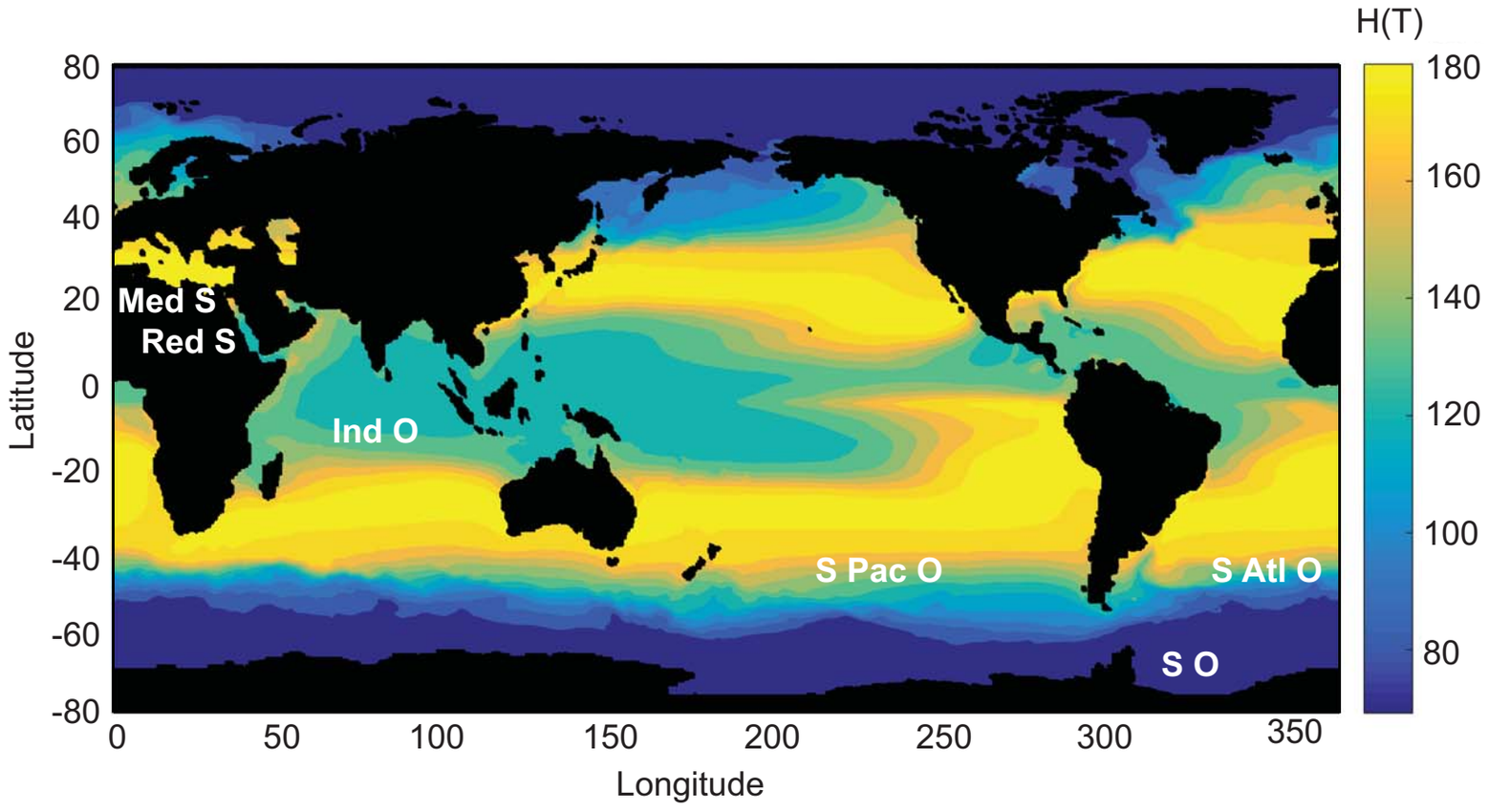
H(T)
180
160
140
120
100
80
Latitude
80
60
40
20
0
-20
-40
-60
-80
Med S
Red S
Ind O
S Pac O
S Atl O
S O
0
50
100
150
200
250
300
350
Longitude

d

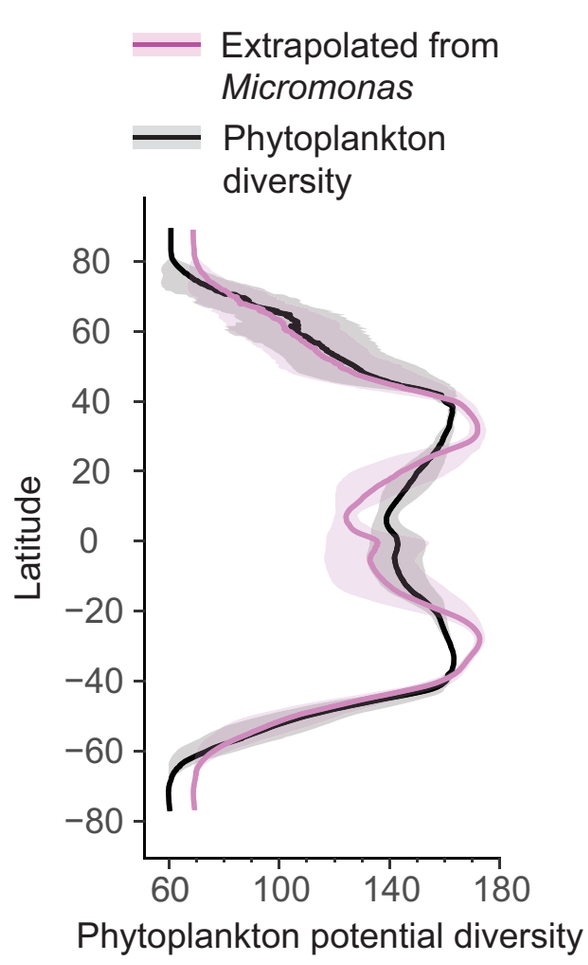
Extrapolated from Micromonas
Phytoplankton diversity
Latitude
80
60
40
20
0
−20
−40
−60
−80
60
100
140
180
Phytoplankton potential diversity

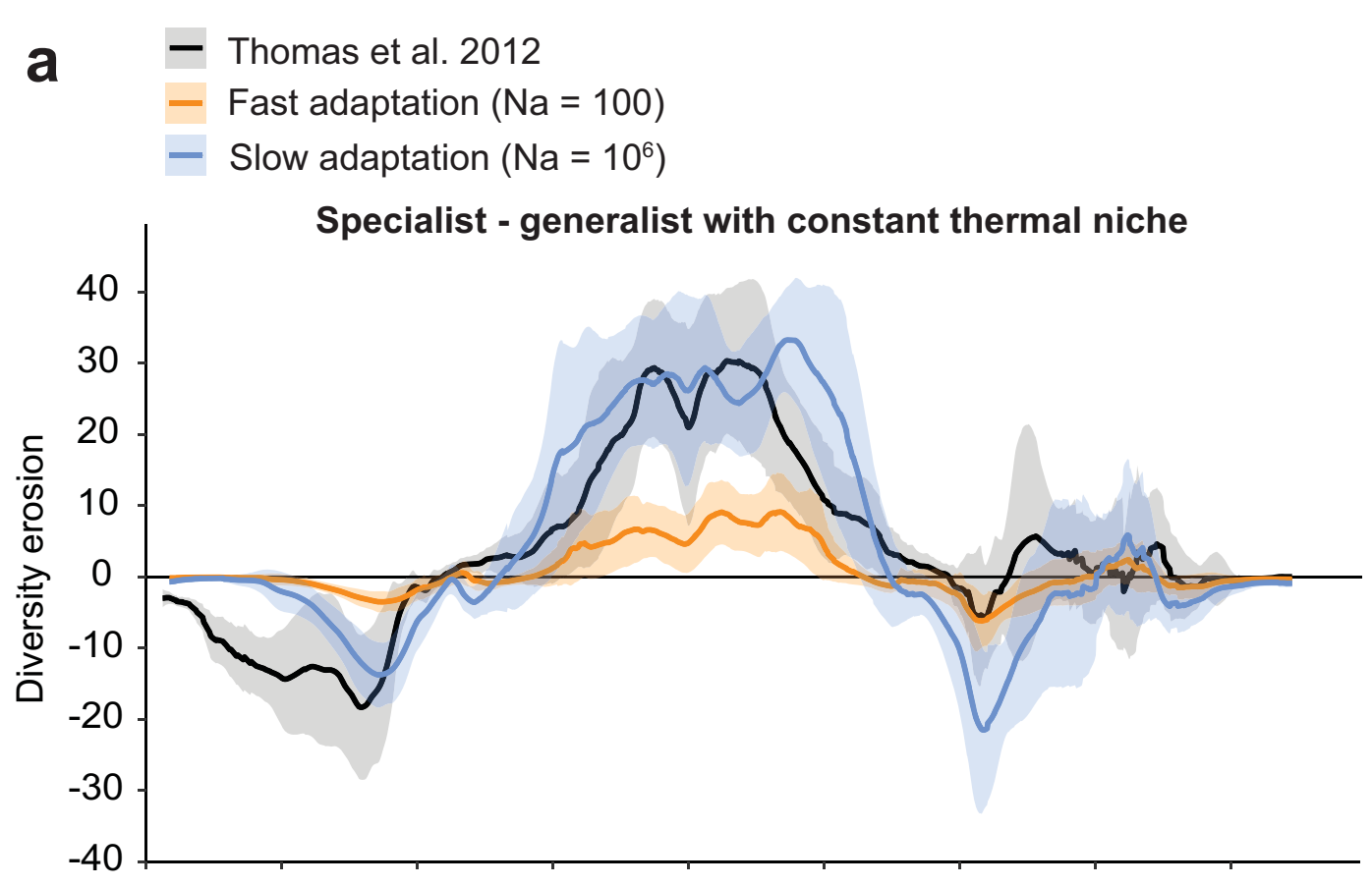
a
Thomas et al. 2012
Fast adaptation (Na = 100)
Slow adaptation (Na = 10⁶)
Specialist - generalist with constant thermal niche
Diversity erosion
40
30
20
10
0
-10
-20
-30
-40

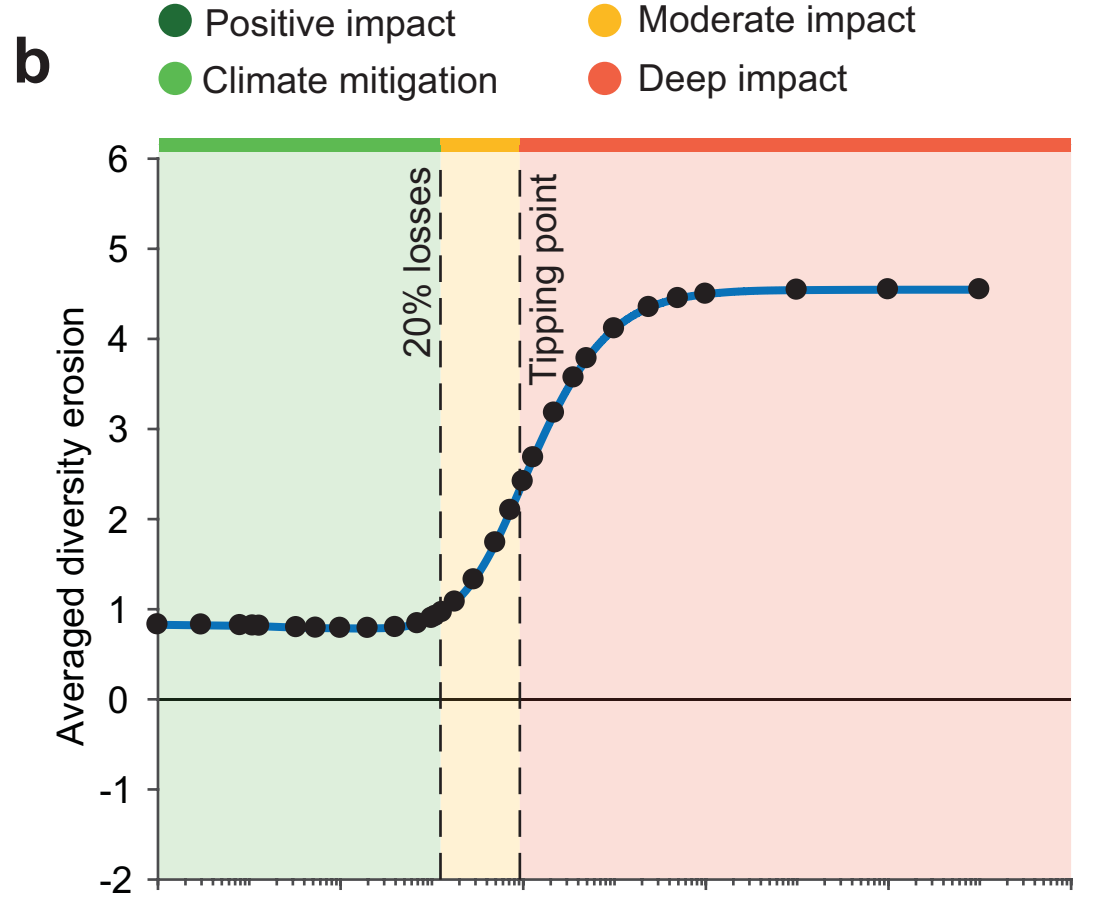
b
Positive impact
Climate mitigation
Moderate impact
Deep impact
20% losses
Tipping point
Averaged diversity erosion
6
5
4
3
2
1
0
-1
-2

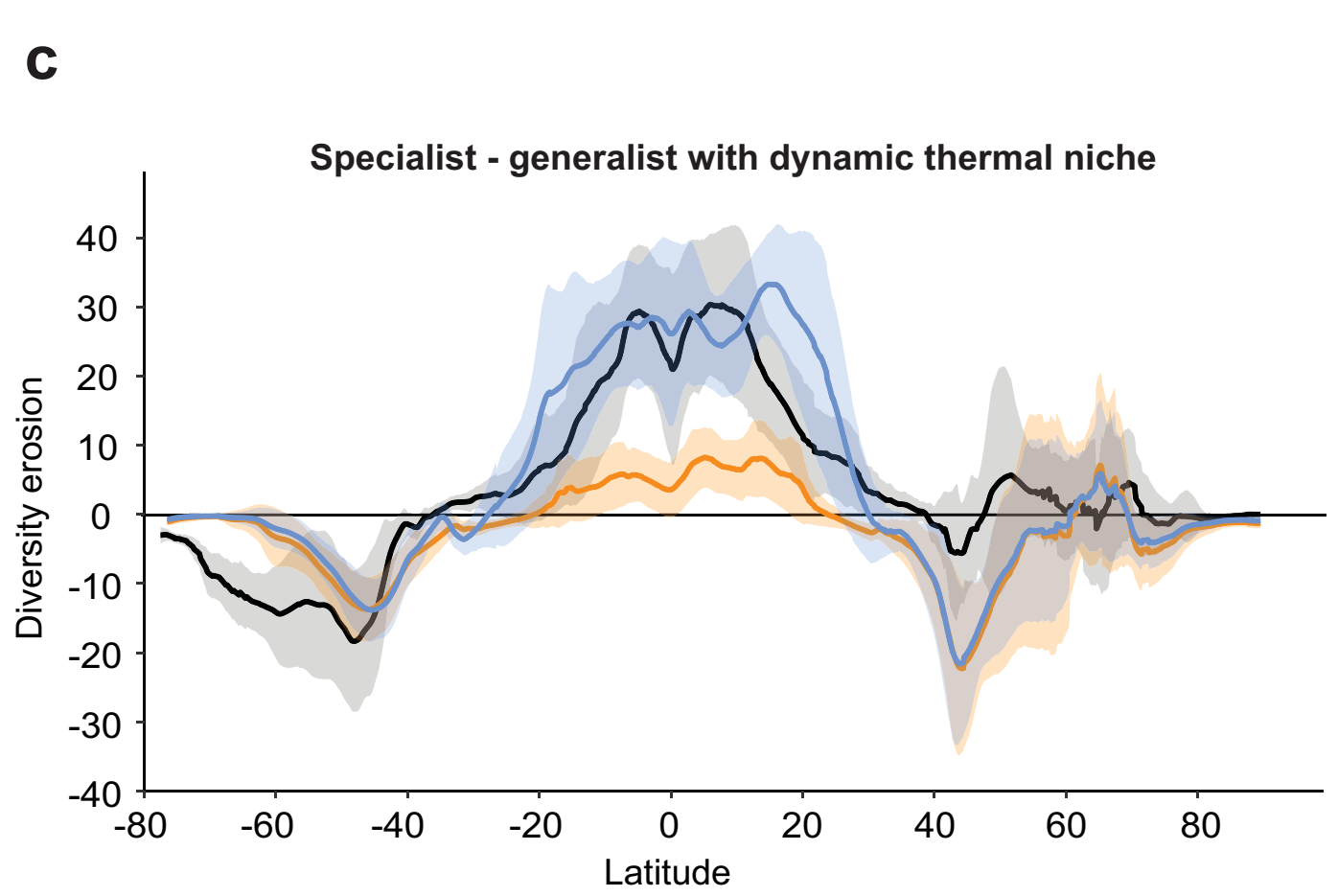
c
Specialist - generalist with dynamic thermal niche
Diversity erosion
40
30
20
10
0
-10
-20
-30
-40
-80
-60
-40
-20
0
20
40
60
80
Latitude

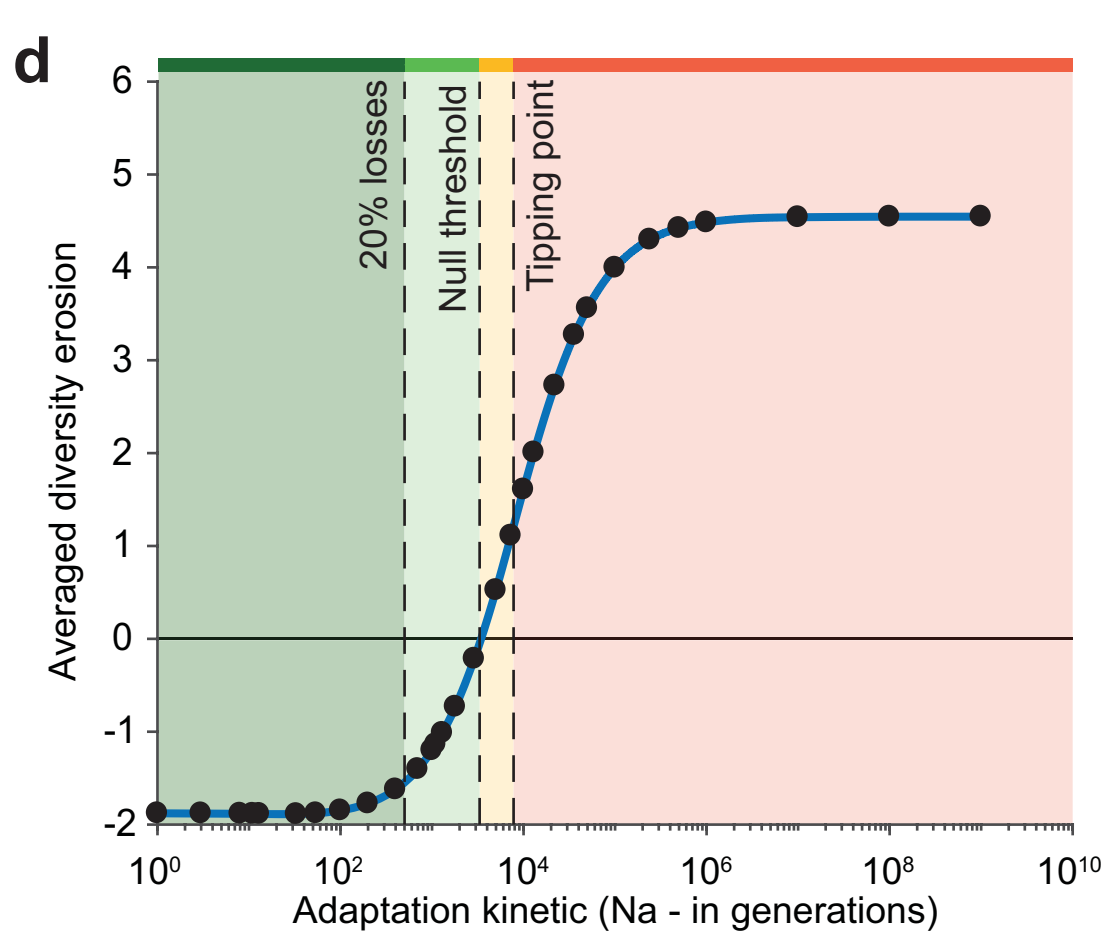
d
20% losses
Null threshold
Tipping point
Averaged diversity erosion
6
5
4
3
2
1
0
-1
-2
10⁰
10²
10⁴
10⁶
10⁸
10¹⁰
Adaptation kinetic (Na - in generations)

Cardinal Parameter	Model	R^2 adjusted	*p*-value
μ_{opt}	$\mu_{opt} = 0.03\overline{T_S} + 0.47$	0.90	$5.68\ 10^{-6}$
T_{max}	$T_{max} = 0.77\overline{T_S} + 17.73$	0.79	0.00014
T_{opt}	$T_{opt} = 0.84\overline{T_S} + 10.24$	0.79	0.00015
T_{min}	$T_{min} = -0.76Lat - 0.92\overline{T_S} + 49.33$	0.47	0.03